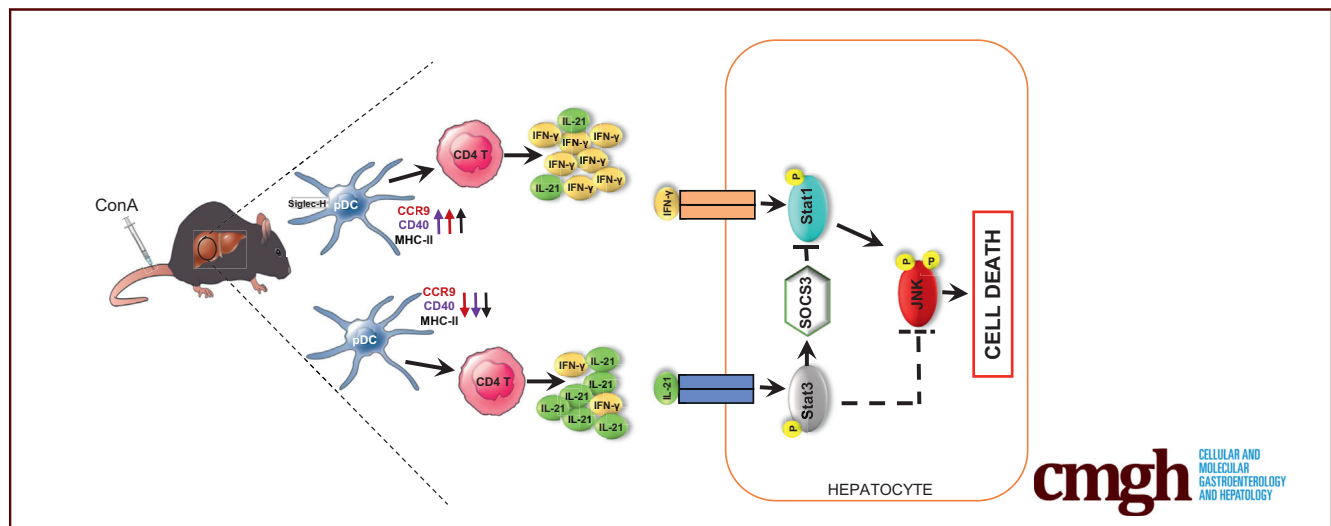


ORIGINAL RESEARCH

Siglec-H^{-/-} Plasmacytoid Dendritic Cells Protect Against Acute Liver Injury by Suppressing IFN- γ /Th1 Response and Promoting IL-21⁺ CD4 T CellsJames Ahodantin,^{1,2} Jiapeng Wu,^{1,3} Masaya Funaki,^{1,2} Jair Flores,^{1,2} Xu Wang,⁴ Pan Zheng,⁵ Yang Liu,⁵ and Lishan Su^{1,2,3,4}

¹Division of Virology, Pathogenesis, and Cancer, Institute of Human Virology, University of Maryland School of Medicine, Baltimore, Maryland; ²Department of Pharmacology, Institute of Human Virology, University of Maryland School of Medicine, Baltimore, Maryland; ³Department of Microbiology and Immunology, Institute of Human Virology, University of Maryland School of Medicine, Baltimore, Maryland; ⁴Division of Immunotherapy, Institute of Human Virology, University of Maryland School of Medicine, Baltimore, Maryland; and ⁵OncoC4, Inc, Rockville, Maryland



SUMMARY

Plasmacytoid dendritic cells were shown to protect against acute liver failure. The present study demonstrated that this protection was enhanced and mediated by interleukin-21-producing CD4 T cells and hyperactivation of Stat3 signaling in the liver of Siglec-H deficient mice.

BACKGROUND & AIMS: Siglec-H is a receptor specifically expressed in mouse plasmacytoid dendritic cells (pDCs), which functions as a negative regulator of interferon- α production and plays a critical role in pDC maturation to become antigen-presenting cells. The function of pDCs in autoimmune and inflammatory diseases has been reported. However, the effect of Siglec-H expression in pDCs in liver inflammation and diseases remains unclear.

METHODS: Using the model of concanavalin A-induced acute liver injury (ALI), we investigated the Siglec-H/pDCs axis during ALI in BDCA2 transgenic mice and Siglec-H^{-/-} mice. Anti-BDCA2 antibody, anti-interleukin (IL)-21R antibody, and Stat3 inhibitor were used to specifically deplete pDCs, block IL21

receptor, and inhibit Stat3 signaling, respectively. Splenocytes and purified naive CD4 T cells and bone marrow FLT3L-derived pDCs were cocultured and stimulated with phorbol myristate acetate/ionomycin and CD3/CD28 beads, respectively.

RESULTS: Data showed that specific depletion of pDCs aggravated concanavalin A-induced ALI. Remarkably, alanine aminotransferase, hyaluronic acid, and proinflammatory cytokines IL6 and tumor necrosis factor- α levels were lower in the blood and liver of Siglec-H knockout mice. This was associated with attenuation of both interferon- γ /Th1 response and Stat1 signaling in the liver of Siglec-H knockout mice while intrahepatic IL21 and Stat3 signaling pathways were upregulated. Blocking IL21R or Stat3 signaling in Siglec-H knockout mice restored concanavalin A-induced ALI. Finally, we observed that the Siglec-H-null pDCs exhibited immature and immunosuppressive phenotypes (CCR9^{Low}CD40^{Low}), resulting in reduction of CD4 T-cell activation and promotion of IL21⁺CD4 T cells in the liver.

CONCLUSIONS: During T-cell-mediated ALI, Siglec-H-null pDCs enhance immune tolerance and promote IL21⁺CD4 T cells in the liver. Targeting Siglec-H/pDC axis may provide a novel approach to modulate liver inflammation and disease. (*Cell Mol*

Gastroenterol Hepatol 2024;18:101367; <https://doi.org/10.1016/j.jcmgh.2024.101367>

Keywords: Siglec-H; Plasmacytoid Dendritic Cells; Inflammation; Hepatic Tolerance.

Liver microenvironment favors the induction of immunologic tolerance to adapt to the continuous exposure to various chemical-derived insults, commensal bacterial products, and pathogens.^{1–3} Dysregulation of intrahepatic immune cell homeostasis can result in hepatic inflammation and acute liver failure (ALF) that is fatal in most individuals.^{4–6} Further investigations are still needed to fully understand the immune components of ALF for effective therapeutic intervention.

Plasmacytoid dendritic cells (pDCs) are a key component of innate immunity. They most efficiently produce the type I interferons (IFN-I) following either toll-like receptor 7 or toll-like receptor 9 engagement by RNA and DNA viruses.^{7–10} Recent studies show that pDCs, after induction of IFN-I, are matured to become antigen-presenting cells (APCs) to prime and stimulate T cells.^{11–13} Furthermore, pDCs contribute to the expansion and differentiation of CD4 T cells into different CD4 T-cell subsets including T helper (Th)1, Th2, and Th17 cells.^{14,15} pDCs can also promote the differentiation of regulatory T cells.^{16–18} Although the involvement of the pDCs/IFN-I axis in chronic inflammatory diseases, such as autoimmune diseases, virus infection, and cancer, has been documented lately,^{19–24} the exact role of pDCs in liver inflammation and disease is still unclear. In a recent report, pDCs was shown to protect against ALF in the concanavalin A (ConA) mouse model of T-cell-mediated hepatitis.²⁵ In addition, Koda et al²⁶ showed that CCR9-null pDCs have a higher efficiency of migration to the liver, resulting in protection against acute liver inflammation.

Sialic acid-binding Ig-type lectin H (Siglec-H [SH]) is a CD33-related Siglec receptor that is expressed by mouse and rat pDCs.^{27,28} In contrast to the other Siglec receptors, SH lacks immunoreceptor tyrosine-based inhibitory motif-like motifs and depends on the presence of the ITAM-containing adaptor 12 (DAP12) for function as a signaling receptor.²⁷ In pDCs, SH can mediate endocytosis and cross-presentation of antigens to promote APC maturation²⁸ and also function as a negative regulator of IFN- α production.²⁷ Recently, SH expression was also detected in other novel subsets of dendritic cells (DC), such as transitional DCs^{29,30} and DC precursors,³¹ which are functionally and transcriptionally distinct from pDCs. In SH-deficient mice, in addition to the enhancement of IFN-I production in pDCs, the loss of SH in pDCs is also associated with a dysregulation of their APC functions.³² However, the exact role of SH/pDCs axis in inflammation and liver injury remains unclear.

In the present study, using the ConA-induced mouse model of T-cell-mediated hepatitis, we demonstrated that the loss of SH led to immunosuppressive pDCs and interleukin (IL)-21-producing CD4 T cells to attenuate acute liver injury (ALI). The protective effect of SH-null pDCs was associated with the inhibition of IFN- γ /Th1 response


mediated by the downregulation of the costimulatory molecule CD40 and the C-C motif chemokine receptor 9 (CCR9) but not IFN-I signaling activation. Furthermore, we show that IL21R blockade or Stat3 inhibition restored ConA-induced ALI in mice lacking SH. Finally, in a coculture model of purified bone marrow (BM) FLT3L-derived pDCs with naive CD4 T cells, we showed that SH deficiency enhances pDC-induced suppression of CD4 T-cell function. These findings indicate that SH-null pDCs enhance immune tolerance in the liver and the induction of IL21/Stat3 signaling pathways contributes to the protection against ConA-induced ALI.

Results

Plasmacytoid Dendritic Cells Protect Against Concanavalin A-Induced Acute Liver Injury

We have recently developed blood dendritic cell antigen 2 (BDCA2) -specific antibody (pDC-dAb or 15B) that specifically and efficiently depletes human pDCs in humanized mice.^{23,24,33} A transgenic mouse strain that expresses human BDCA2 on all mouse pDCs has been established to specifically target pDCs in mice.^{34,35} First, over a year of monitoring, we did not observe or detect any spontaneous health concerns including liver disease in naive BDCA2 transgenic mice (data not shown). To clarify the role of pDCs in ALI, we investigated the effect of pDCs depletion on ALI using the mouse model of ConA-induced T-cell-mediated ALI. To specifically deplete pDCs, BDCA2 transgenic mice were administered with pDC-dAb followed by ConA injection 24 hours later (Figure 1A). Compared with isotype control group, more than 50% reduction in pDCs levels was observed in the liver and spleen at 36 hours of pDC-dAb administration (Figure 1B and C). The measurement of alanine aminotransferase (ALT) and hyaluronic acid (HA), surrogate blood markers of liver injury, showed similar ALT and HA levels in the blood of mice with isotype and pDC-dAb, indicating that pDC-dAb itself did not induce liver injury. However, we observed higher ALT and HA levels in the blood of ConA-treated animals with pDCs depletion compared with control animals (Figure 1D and E). Similarly, the examination of liver tissues revealed that pDCs depletion alone did not affect liver conditions, whereas combination with ConA led to remarkably higher liver injury and

Abbreviations used in this paper: ALF, acute liver failure; ALI, acute liver injury; ALT, alanine aminotransferase; APCs, antigen-presenting cells; BDCA2, blood dendritic cell antigen 2; BM, bone marrow; CCR9, C-C motif chemokine receptor 9; ConA, concanavalin A; CXCL-10, C-X-C motif chemokine ligand 10; DAP12, DNAX-activation protein 12; DCs, dendritic cells; FLT3L, Fms-related tyrosine kinase 3 ligand; HA, hyaluronic acid; IFN, interferon; IHL, intrahepatic leukocytes; IL, interleukin; JNK, c-Jun N-terminal kinases; KO, knockout; MHC, major histocompatibility complex; PBS, phosphate-buffered saline; PCR, polymerase chain reaction; pDC-dAb, pDC depletion antibody; pDCs, plasmacytoid dendritic cells; Siglec, sialic acid-binding Ig-type lectin; SOCS, suppressor of cytokine signaling; STAT, signal transducer and activator of transcription; Th, T helper; WT, wild type.

 Most current article

© 2024 The Authors. Published by Elsevier Inc. on behalf of the AGA Institute. This is an open access article under the CC BY-NC-ND license (<http://creativecommons.org/licenses/by-nc-nd/4.0/>).

2352-345X

<https://doi.org/10.1016/j.jcmgh.2024.101367>

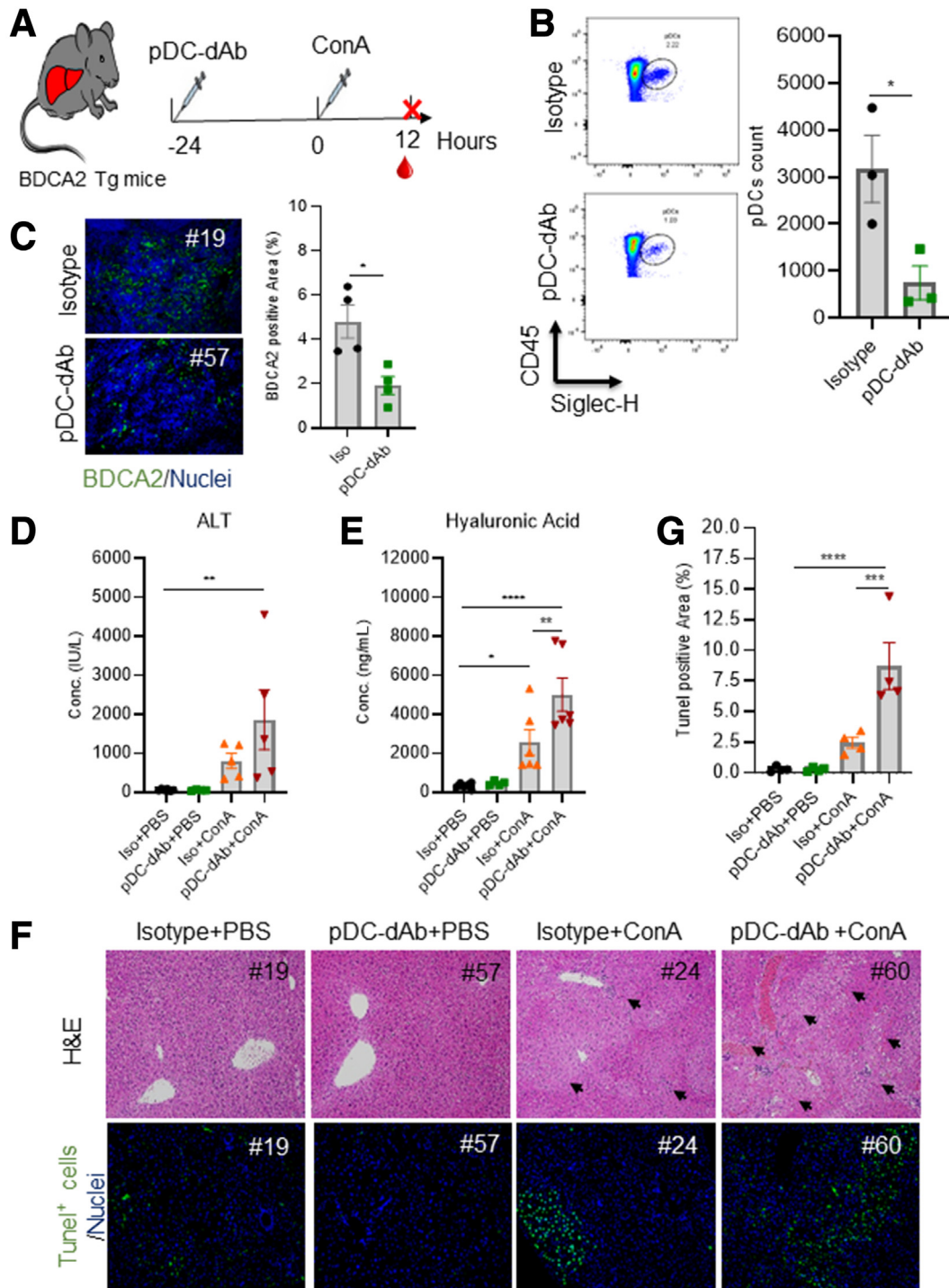


Figure 1. pDCs protect against ConA-induced acute liver injury. (A) Experiment design: BDCA2 transgenic mice were treated with pDC-dAb or isotype control and euthanized 12 hours after ConA injection. (B) Representative FACS plots and pDCs count in the liver of BDCA2 Tg mice administrated with isotype or pDC-dAb. (C) Immunofluorescence staining for BDCA2/CD303 (green) in the spleen and its quantification by ImageJ. Enzyme-linked immunosorbent assay detection of (D) ALT and (E) HA in the animals' blood at 12 hours post-ConA. (F) Hematoxylin and eosin (H&E) staining (top) and detection of apoptotic cells (green, bottom) by TUNEL assay, and (G) ImageJ quantification of TUNEL-positive area in liver sections of pDC-dAb- and isotype-treated SH KO at 12 hours post-ConA injection. All images were acquired with $\times 20$ magnification lens. Bars in the histograms represent the standard error of the mean. Statistical analysis was performed with 2-way analysis of variance (ANOVA) and Tukey post hoc test; * $P < .05$; ** $P < .005$; *** $P < .0005$; **** $P < .00005$.

hepatocytes death (Figure 1F and G). Altogether, these data indicate that pDCs play a protective role in ConA-induced ALI, consistent with data in a previous report.²⁵

Siglec-H Deficiency Attenuates Concanavalin A-Induced Acute Liver Injury Correlates with IL21 and Stat3 Signaling Pathways Activation

As a modulator of pDC activity, SH is specifically expressed in mouse pDCs (Figures 2 and 3).^{27,28} It has been

reported that SH-null pDCs produce more IFN- α on CpG oligodeoxynucleotides stimulation and have a reduced ability in priming of CD4 and CD8 T cells in lymphoid tissues.^{32,36} To elucidate the role of the SH/pDCs axis in ALI and the associated mechanism, SH^{-/-} (SH knockout [KO]) and wild-type (WT) mice were administrated with ConA as described previously (Figure 4A). First, SH deficiency alone did not induce any spontaneous hepatic disease during the time course of this study or over 12 months of monitoring (data not shown). Liver tissues from naive WT and SH KO

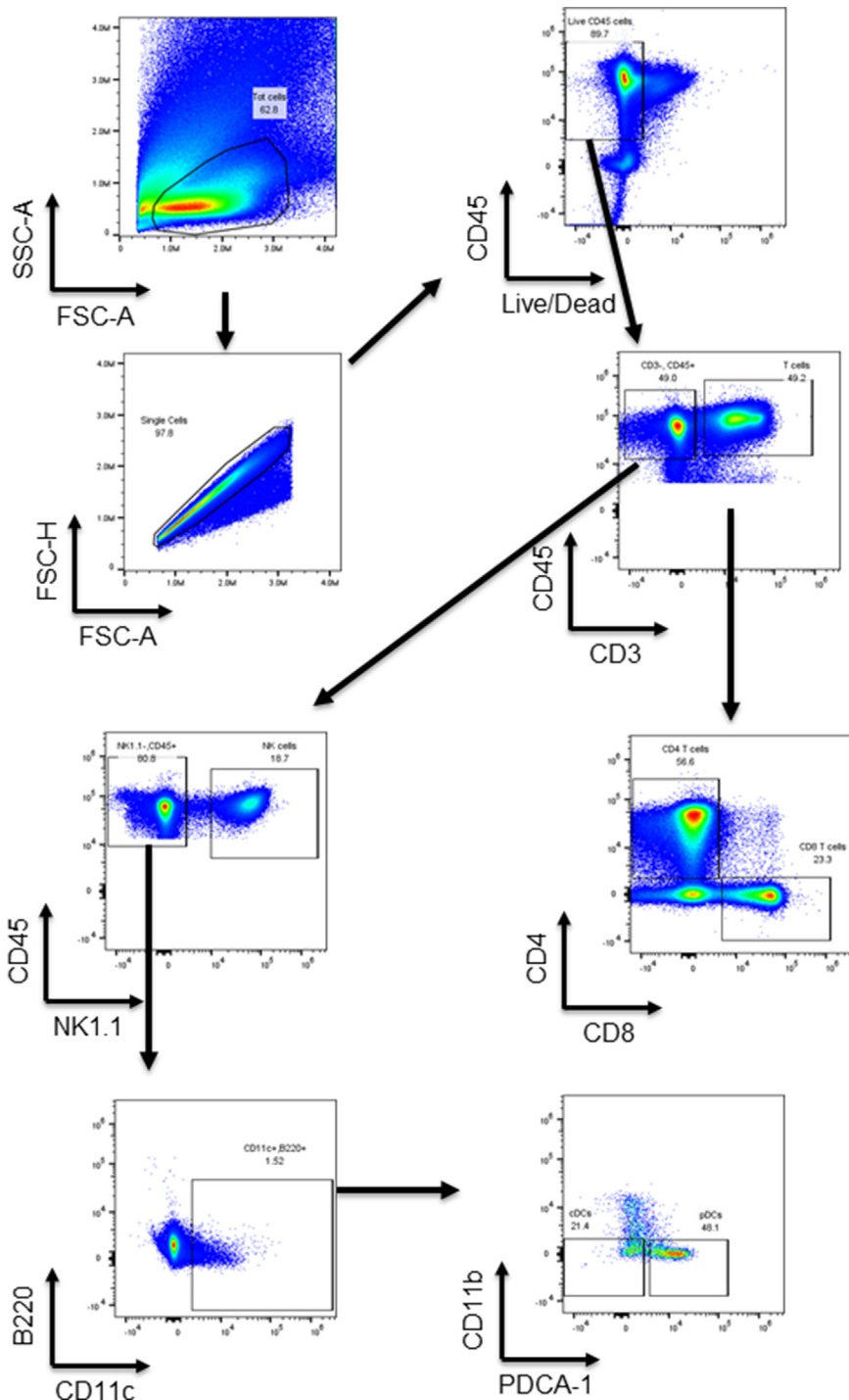


Figure 2. Flow cytometry gating strategy of IHL.

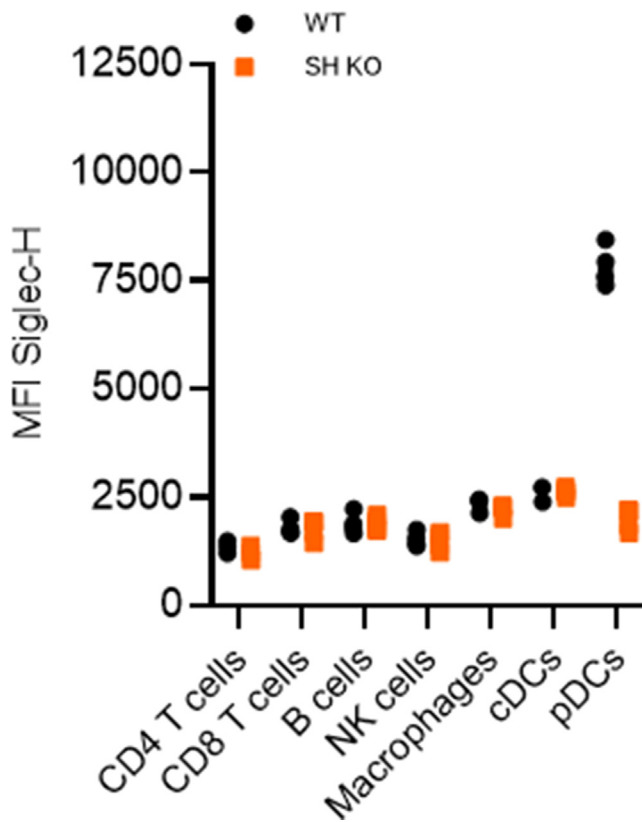


Figure 3. SH expression patterns in intrahepatic immune subsets. Mean fluorescence intensity (MFI) of SH in different subsets of IHL from naive WT and SH KO mice detected by flow cytometry.

mice were similar after a macroscopic analysis (light brown liver) (Figure 4B). Following ConA administration, compared with WT mice (dark brown liver), liver from SH KO mice showed less damage (brown liver) (Figure 4B) with no significant difference in the percentage of liver over body weight between different groups (data not shown). Moreover, ConA-treated SH KO mice presented lower blood levels of ALT, HA, and proinflammatory cytokines IL6 and tumor necrosis factor- α (Figure 4C–F). Consistently, hematoxylin and eosin and TUNEL assays with liver section staining revealed less liver damage and reduced dead hepatocytes in SH KO mice when compared with WT mice after ConA administration (Figure 4G and H).

ConA-induced hepatitis and ALI is reported to be mediated by CD4 T-cell-induced IFN- γ and the activation of Stat1 signaling pathway.³⁷ We thus analyzed components of those pathways in the liver. First, consistent to data obtained in the blood, intrahepatic proinflammatory cytokines IL6 and tumor necrosis factor- α expression levels were lower in SH KO mice compared with WT mice after ConA (Figure 5A and B). Moreover, ConA administration induced a significant increase in transcription levels of transforming growth factor- β , IFN- γ , interferon regulatory factor 1, and CXCL-10 in WT mice, whereas the levels of those markers were significantly reduced in SH KO mice (Figures 5C–E and 6A). However, the suppressor of cytokine signaling-3 (SOCS3)

mRNA was similarly upregulated in the liver of both ConA-treated groups compared with phosphate-buffered saline (PBS)-mice (Figure 5F). Although, there was no difference in intrahepatic levels of IL1 β , IL4, IL5, IL12a, IL15, IL17, and ISG-15 between both treated groups (Figure 6B–H), we did observe an enhancement of IFN- β , OAS1, and IL21 expression levels in the liver of SH-deficient mice compared with WT animals with ConA treatment (Figures 5G and H and 6I). These data indicate that alleviation of ConA-induced ALI by SH deficiency correlated with elevation of IFN- β /OAS1 and IL21 expressions in the liver.

To determine related changes in signaling pathways involved in ConA-induced ALI, we further analyzed liver protein extracts by immunoblots. We detected a decrease of the phosphorylated Stat1 and JNK proteins, and a higher phosphorylated Stat3 protein in SH-null livers (Figures 5I–L and 7A). The reduction of Stat1 signaling activation in the liver of SH KO mice suggested that IFN- β /OAS1 signaling was not involved and that the attenuation of ALI observed with SH loss was likely mediated by the activation of Stat3 signaling pathway via elevated IL21.^{38–40}

Taken together, these results showed that SH-deficient pDCs led to inhibition of IFN- γ and Stat1 signaling pathways and elevation of IL21 and Stat3 signaling pathways, resulting in the mitigation of ConA-induced liver inflammation and damage.

Blocking IL21R and Stat3 Signaling Pathways Restores Concanavalin A-Induced Liver Injury in Siglec-H^{-/-} Mice

To further define the protective effect of IL21/Stat3 signaling in SH^{-/-} mice, we performed a blocking or inhibition of IL21 and Stat3 signaling pathways in SH-deficient mice followed by injection of ConA and evaluated the ALI levels (Figure 8A). Interestingly, both anti-IL21R antibody and Stat3 inhibitor (HJC-0416) treatments led to higher ALT and HA levels compared with ConA alone (Figure 8B and C). Consistently, hematoxylin and eosin and TUNEL staining of liver tissues revealed elevated levels of liver damage and hepatocyte death in ConA-treated SH-KO mice with either IL21 blockade or Stat3 inhibition (Figure 8D and E). Furthermore, anti-IL21R- and HJC-046-treated SH KO mice showed a reduced level of Stat3 phosphorylation and an enhancement of ConA-induced JNK phosphorylation in the liver of SH KO mice (Figure 8F–H).

Altogether, these results demonstrate that SH-deficient pDCs attenuated ConA-induced ALI in vivo through an inhibition of IFN- γ /Th1 response and an increase of IL21 production that promotes Stat3 signaling activation.

Loss of Siglec-H Expression Induces Tolerogenic Plasmacytoid Dendritic Cells

Herein, we investigated the impact of SH loss in pDCs on their APC functions in the liver and how this might contribute to the attenuation of ConA-induced ALI. For that, intrahepatic leukocytes (IHL) isolated from naive WT and SH KO mice were phenotyped using flow cytometry. The analysis of pDCs from naive livers showed and confirmed

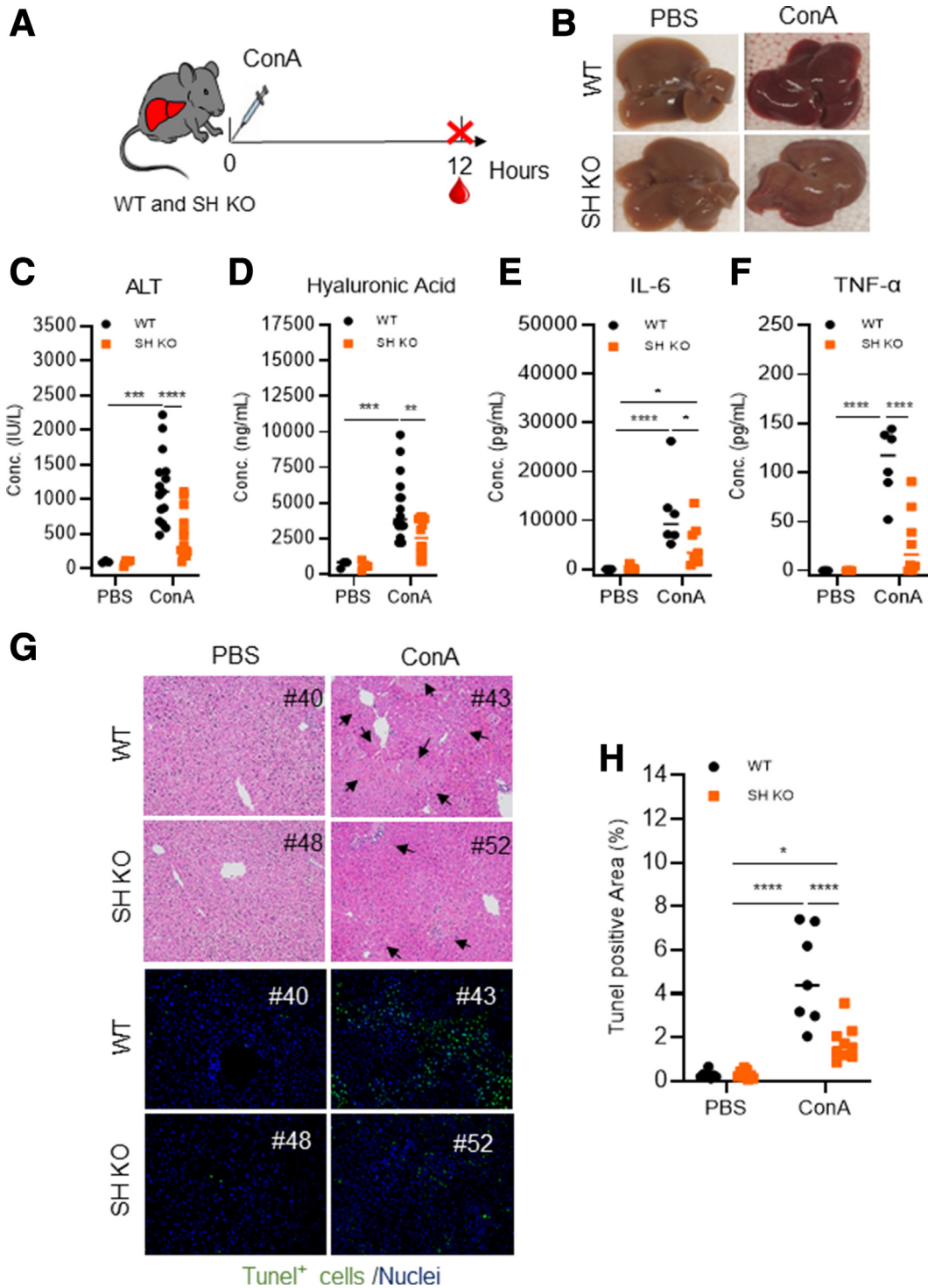


Figure 4. SH deficiency protects against ConA-induced acute liver injury. (A) Experiment design: WT and SH KO mice were injected intravenously with 15 mg/kg ConA and euthanized 12 hours later. (B) Photographs of liver of WT and SH KO mice treated with ConA and PBS. Enzyme-linked immunosorbent assay detection of (C) ALT, (D) HA, (E) IL6, and (F) tumor necrosis factor (TNF)- α in the blood of animals at 12 hours after ConA and PBS injections. (G) Hematoxylin and eosin (H&E) staining (*top*), and detection of apoptotic cells (*green*) with nuclei (*blue*) by TUNEL assay (*bottom*), and (H) ImageJ quantification of TUNEL-positive area in the liver sections of animals at 12 hours after ConA and PBS injections. *Arrows* indicate liver lesions. All images were acquired with $\times 20$ magnification lens. *Bars* in the scatter plots represent the median value. Statistical analysis was performed with 2-way ANOVA and Tukey post hoc test; * $P < .05$; ** $P < .005$; *** $P < .0005$; **** $P < .00005$.

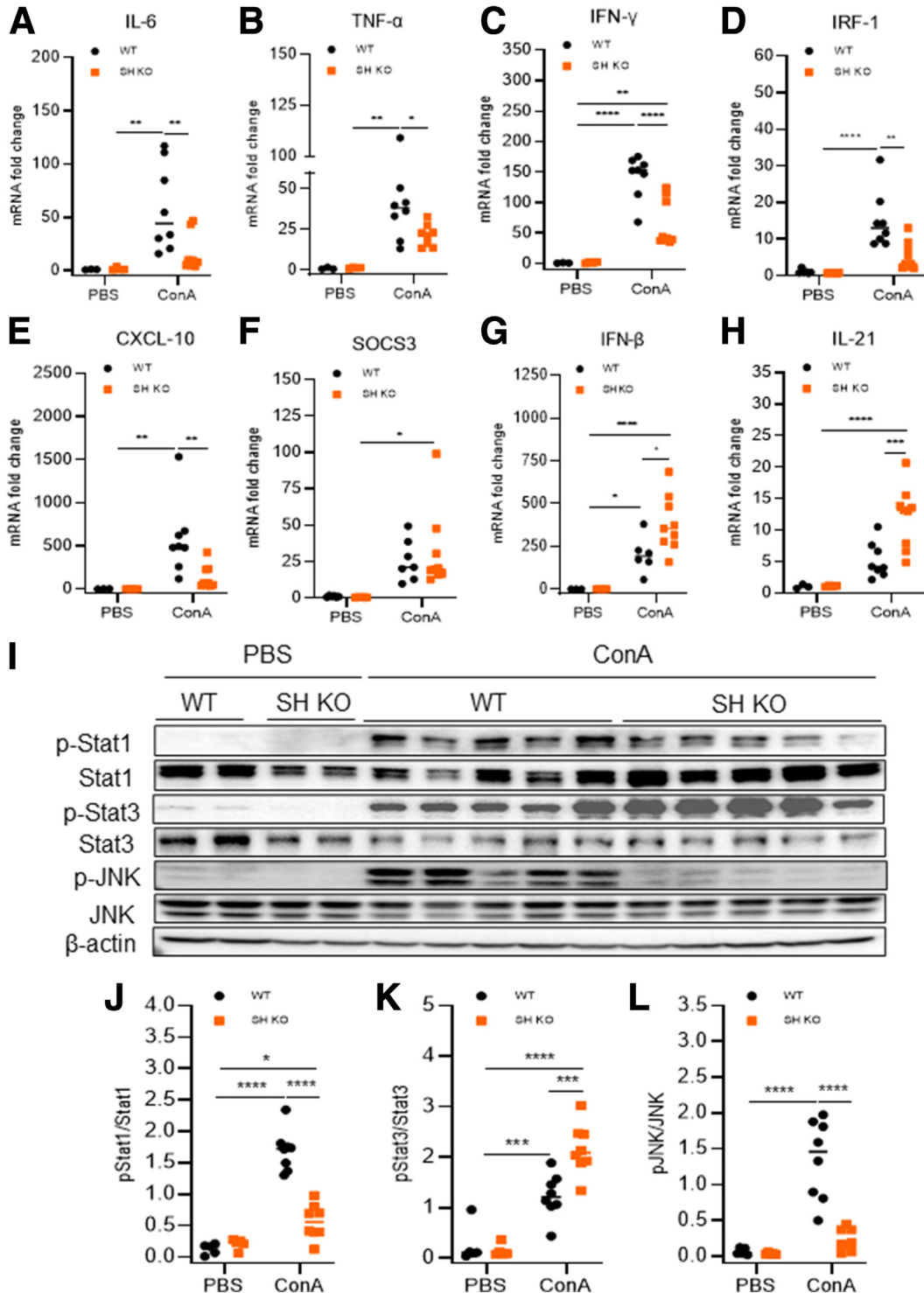


Figure 5. Loss of SH prevents ConA-induced IFN- γ /Stat1 and JNK signalings activation and enhances Stat3, IFN-I, and IL21 levels in the liver. mRNAs and proteins were isolated from WT and SH KO mice livers 12 hours after ConA injection for analysis. Intrahepatic expression levels of mRNA of (A) IL6, (B) TNF- α , (C) IFN- γ , (D) interferon regulatory factor 1 (IRF-1), (E) CXCL-10, (F) SOCS3, (G) IFN- β , and (H) IL21 analysis by real-time quantitative PCR. (I-L) Immunoblot detection and quantification of anti-phospho- Stat1, Stat3, JNK, and their corresponding total isoforms, and β -actin. Target proteins quantification was performed with ImageJ and presented as ratio phosphorylated over total isoforms. Bars in the scatter plots represent the median value. Statistical analysis was performed with 2-way ANOVA and Tukey post hoc test; * $P < .05$; ** $P < .005$; *** $P < .0005$; **** $P < .00005$.

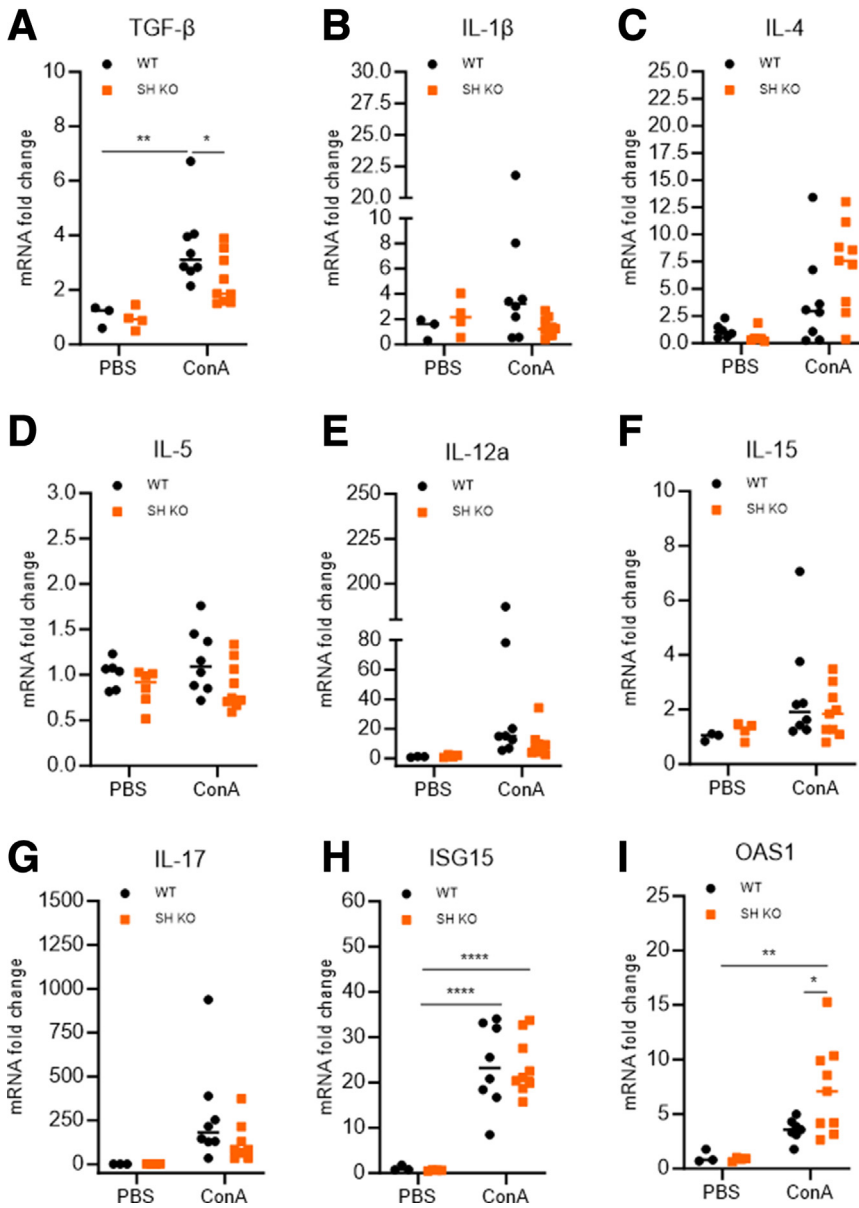
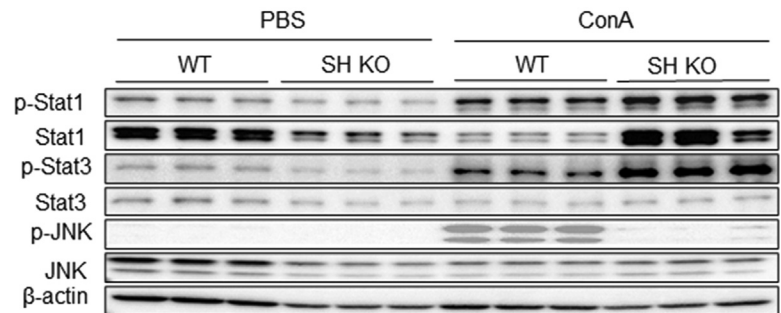


Figure 6. Modulation of intrahepatic cytokines in ConA-treated WT and SH KO mice. Inflammation and interferon signaling related genes were assessed in the liver by real-time quantitative PCR, 12 hours of PBS or ConA administration to animals. Intrahepatic levels of (A-G) TGF- β , IL1 β , IL4, IL5, IL12a, IL15, IL17, and IFN-stimulated genes (H, I) ISG15 and OAS1. Bars in the scatter plots represent the median value. Statistical analysis was performed with 2-way ANOVA and Tukey post hoc test; * $P < .05$; ** $P < .005$; *** $P < .0005$; **** $P < .00005$.

Figure 7. Signaling pathways in ConA-induced acute liver injury in WT and SH KO mice. Proteins were isolated from WT and SH KO mice livers 12 hours after ConA injection for analysis. Immunoblot detection and quantification of anti-phospho- Stat1, Stat3, JNK, and their corresponding total isoforms, and β -actin. Target proteins quantification was performed with ImageJ and presented as ratio phosphorylated over total isoforms. Quantification data were combined and presented in Figure 5.



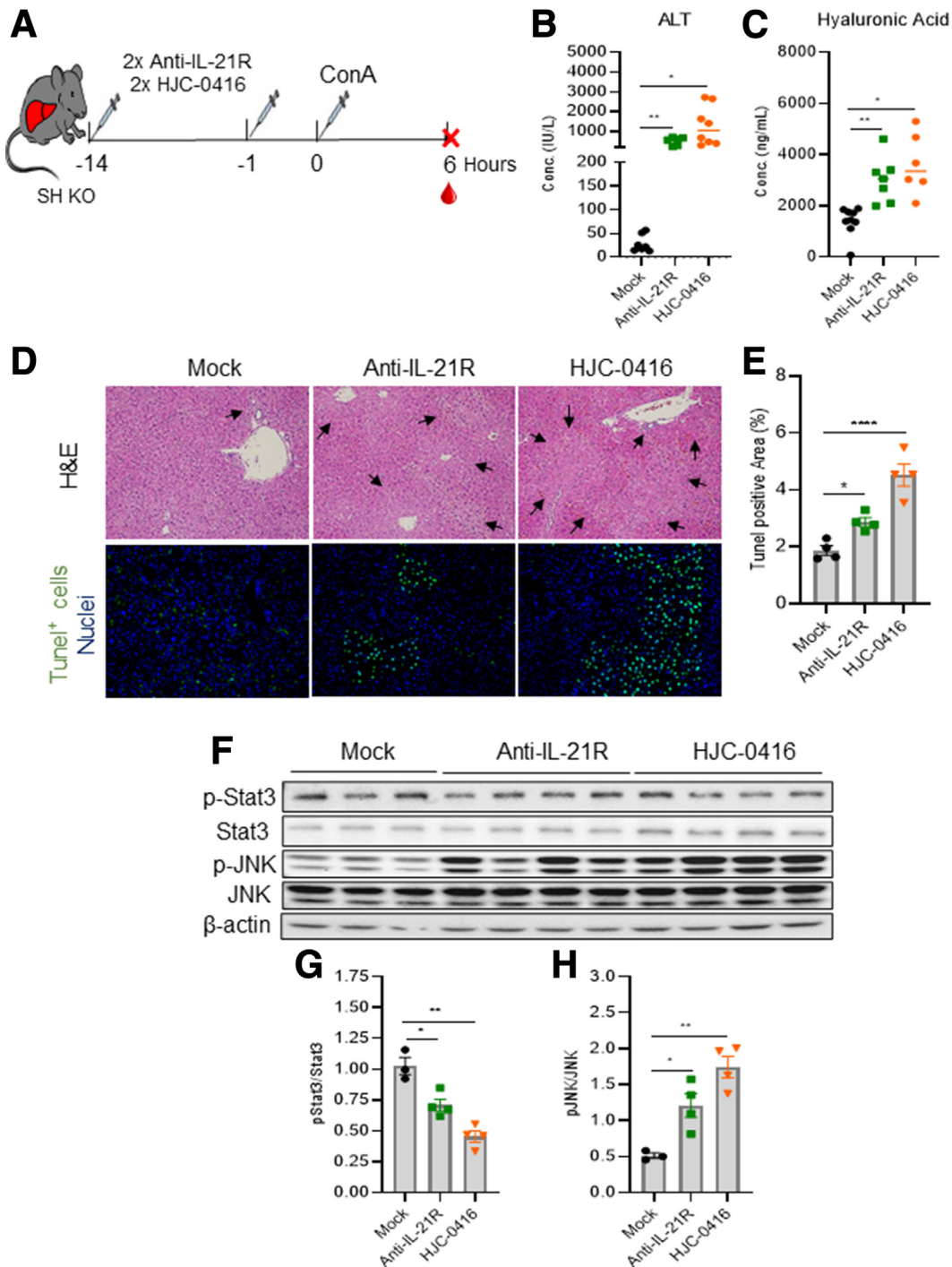


Figure 8. IL21R and Stat3 blockade restores ConA-induced acute liver injury in SH-deficient mice. (A) Experiment design: SH KO mice treated with either anti-IL21R antibody or HJC-0416 (Stat3 inhibitor) and terminated 6 hours after ConA administration. Enzyme-linked immunosorbent assay detection of (B) ALT and (C) HA in the blood at 6 hours post-ConA injection. (D) H&E staining (top), and detection of apoptotic cells (green) with nuclei (blue) by tunnel assay (bottom) in liver sections of anti-IL21R- and HJC-0416-treated SH KO at 6 hours post-ConA injection, and (E) ImageJ quantification of tunnel positive area. All images were acquired with $\times 20$ magnification lens. (F-H) Immunoblot detection and quantification of anti-phospho Stat3 (G) and JNK (H), and their corresponding total isoforms. Target proteins quantification was performed with ImageJ and presented as ratio phosphorylated over total isoforms. Bars in the scatter plots and histograms represent the median value and the SEM respectively. Statistical analysis was performed with 2-tailed unpaired *t* test; **P* < .05; ***P* < .005; ****P* < .0005; *****P* < .00005.

that SH expression is restricted to pDCs (Figures 2 and 3), and its loss was associated with a downregulation of major histocompatibility complex (MHC)-II, CD86, and CCR9 molecules (Figure 9A–C). In addition, we also detected a significant reduction in the amounts of the costimulatory molecule CD40 in naive liver's pDCs from SH KO mice compared with WT pDCs (Figure 9D). This was consistent with observations previously reported in SH-null pDCs from lymphoid tissues.^{32,41}

Next, we performed a similar analysis of pDCs in the context of ConA-induced ALI. Although the IHL CD45⁺ cells number was similar among all animals (Figure 10A), we observed about 50% reduction in the number of liver's pDCs within 6 hours of ConA administration compared with mice receiving PBS (Figure 10B and C), suggesting that ConA itself induced a depletion of pDCs in the liver through an unclear mechanism. However, the expression of SH on liver's pDCs remained unchanged among all groups, indicating that ConA treatment did not affect SH expression in liver's pDCs (Figure 10D). Following ConA injection, MHC-II molecules were upregulated in both pDCs from WT and SH-KO mice livers but remained lower in pDCs from SH KO livers (Figure 11A). However, CD86 molecules were similarly elevated in liver's pDCs of treated mice compared with mice with PBS (Figure 11B). Interestingly, we observed that ConA administration enhanced the expression of both CD40 and CCR9 in WT liver's pDCs, whereas their expression levels in pDCs from SH KO livers remained significantly low (Figures 10E and F and 11C and D). The expression of all these molecules were unchanged in intrahepatic cDCs (Figure 12) or monocytes and macrophages (data not shown) from both treated groups. Altogether, these findings reveal that besides its inhibitory effect on IFN-I production in pDCs,^{32,36} SH regulates key molecules involved in APC functions of pDCs and its deficiency promotes pDCs with immunosuppressive features.

Siglec-H-Null pDCs Suppress CD25⁺CD4⁺ T-Cell Activity and Promote IL21 Production During Acute Liver Injury

Next, we analyzed the effect of SH-null pDCs on T-cell activation during ConA-induced ALI. First, similar total T cells including CD4 and CD8 T cell numbers were detected in IHL of all animals (Figure 13A–C). As expected, ConA administration promoted intrahepatic accumulation of CD25⁺ CD4 T cells and CD25⁺ CD8 T cells in WT mice. Interestingly, the number of CD25⁺ CD4 T cells in the liver of SH KO mice treated with ConA was significantly lower compared with WT counterpart (Figure 13D–G). The number of CD25⁺ CD8 T cells was also slightly lower in the liver of SH KO mice after treatment but did not reach significance (Figure 13H and I).

To further define the role of IL21 and Stat3 signaling in ConA-induced ALI in SH deficient mice, IFN- γ and IL21 expression levels were measured in IHL by quantitative polymerase chain reaction (PCR) and T-cell functional assay ex vivo. Unlike IHL from WT mice, IFN- γ transcripts were not induced in IHL from SH KO mice after ConA

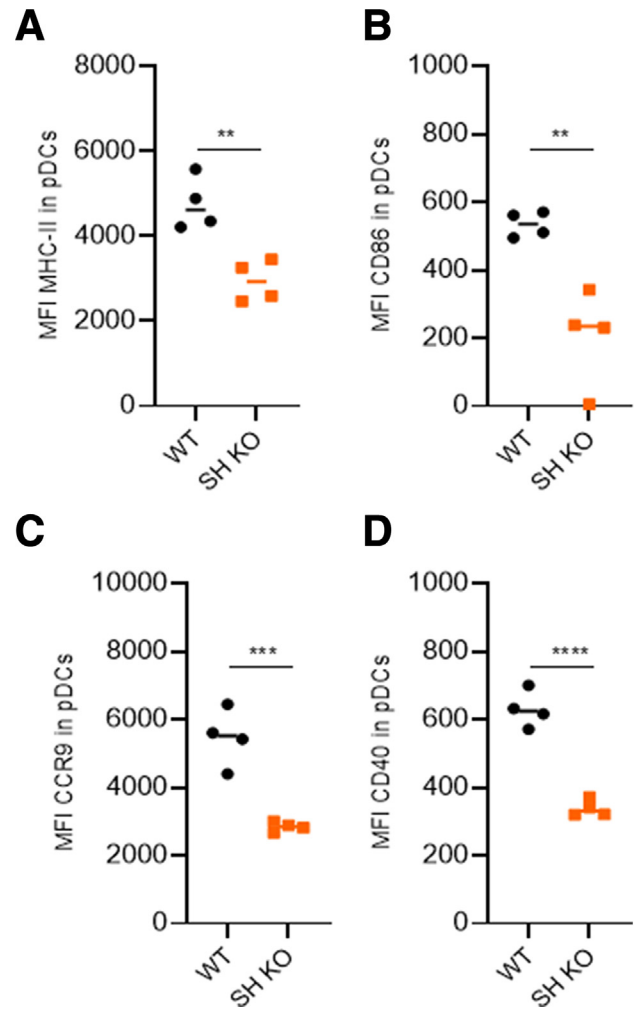


Figure 9. SH loss in pDCs affects molecules associated with APC functions. Mean fluorescence intensity (MFI) of (A) MHC-II, (B) CD86, (C) CCR9, and (D) CD40 in pDCs isolated from the liver of naive WT and SH KO mice. Bars in the scatter plots represent the median value. Statistical analysis was performed with 2-tailed unpaired *t* test; **P* < .05; ***P* < .005; ****P* < .0005; *****P* < .00005.

administration (Figure 14A) but they showed a significant augmentation of IL21 expression levels (Figure 14B). ConA treatment did not induce the expression of IFN- β and OAS1 in IHL (data not shown). Furthermore, ex vivo stimulation of T cells with phorbol myristate acetate and ionomycin showed lower IFN- γ ⁺ CD4 T cells and increased IL21⁺ CD4 T cells in SH-deficient mice (Figure 14C–F). We did not observe such differences in CD8 T cells after stimulation (Figure 15). This suggests that SH-null pDCs affect mainly the activation of CD4 T cells in the liver.

Finally, we performed CD4 T cells and pDCs coculture in vitro to better characterize the suppressive effect of pDCs and its modulation by SH loss. For that, purified CD25⁺CD4⁺ T cells from the spleen of WT mice were cocultured with BM FLT3L-derived pDCs from WT and SH KO mice and stimulated or not with CD3/CD28 beads. Consistently, compared with stimulated CD4 T cells alone, addition of WT pDCs led

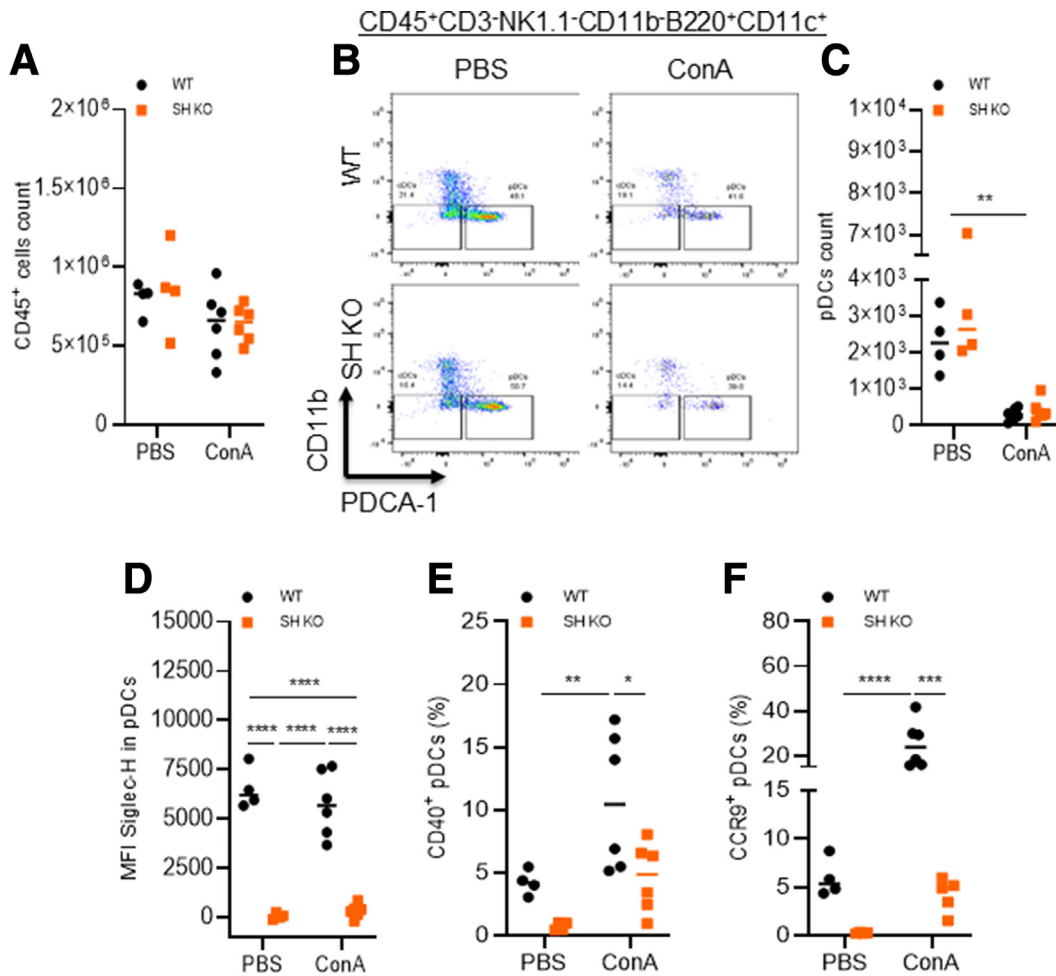


Figure 10. ConA fails to induce CD40 and CCR9 expressions in SH-null pDCs. IHL were isolated from WT and SH KO mice 6 hours after PBS/ConA administration and analyzed by flow cytometer. (A) CD45⁺ cells number in the liver. (B, C) Representative FACS plots and summary of intrahepatic pDCs count determined by flow cytometer. (D) MFI of SH in pDC. (E, F) Frequencies of CD40 and CCR9 in pDCs isolated from the liver. Bars in the scatter plots represent the median value. Statistical analysis was performed with 2-way ANOVA and Tukey post hoc test; * $P < .05$; ** $P < .005$; *** $P < .0005$; **** $P < .00005$.

to a reduction of CD25⁺, CD69⁺, and double positive (CD25⁺CD69⁺) CD4 T cells, which frequencies were further lowered by SH KO pDCs (Figure 16A–F). Intriguingly, compared with stimulated T cells alone condition, IFN- γ amounts in supernatants were similarly reduced by WT and SH KO pDCs (Figure 16G) and IL21 remained undetectable in the supernatants by enzyme-linked immunosorbent assay (Figure 16H). These findings revealed that during acute inflammation, SH loss in pDC enhances pDC-induced suppression of CD4 T cells activation.

Discussion

It has been reported that pDCs play an important role in chronic liver disease.^{20,42–44} However, the exact role of intrahepatic pDCs in the pathogenesis of ALI/ALF is unclear and the associated mechanism is still elusive. Here, we deciphered the role of SH in pDCs in ALI. First, we showed that specific depletion of pDCs exacerbated T-cell-mediated ALF (Figure 1), indicating that hepatic pDCs protect against ALI as previously reported.²⁵ Importantly, the present study

revealed that SH deficiency in pDCs fostered immature pDCs (CD86^{Low}MHC-II^{Low}CCR9^{Low}CD40^{Low}) with tolerogenic features pDCs to attenuate inflammation in the liver through the diminution of activated intrahepatic CD4 T cells. Additionally, we demonstrated that these tolerogenic pDCs dampened IFN- γ /Th1 response and promoted IL21-producing CD4 T cells to attenuate ConA-induced T-cell-mediated hepatitis and hepatocytes death. These findings indicate that, during T-cell-mediated hepatitis and liver injury, SH-null pDCs mediate hepatic tolerance via induction of IL21⁺ CD4 T cells in the liver. Targeting SH in pDC may provide a novel approach to modulate CD4 T-cell polarization and liver disease.

Intriguingly, IFN- β and IL21 were upregulated in the liver of SH-null mice after ConA administration (Figure 5G and H). We thus hypothesized that Stat3 signaling pathway activation and the alleviation of ALI could be mediated by either 1 or both IFN- β and IL21 produced by activated IHL. Indeed, SH has been reported to negatively regulate IFN-I production in pDCs.^{32,36} Besides its well-documented role

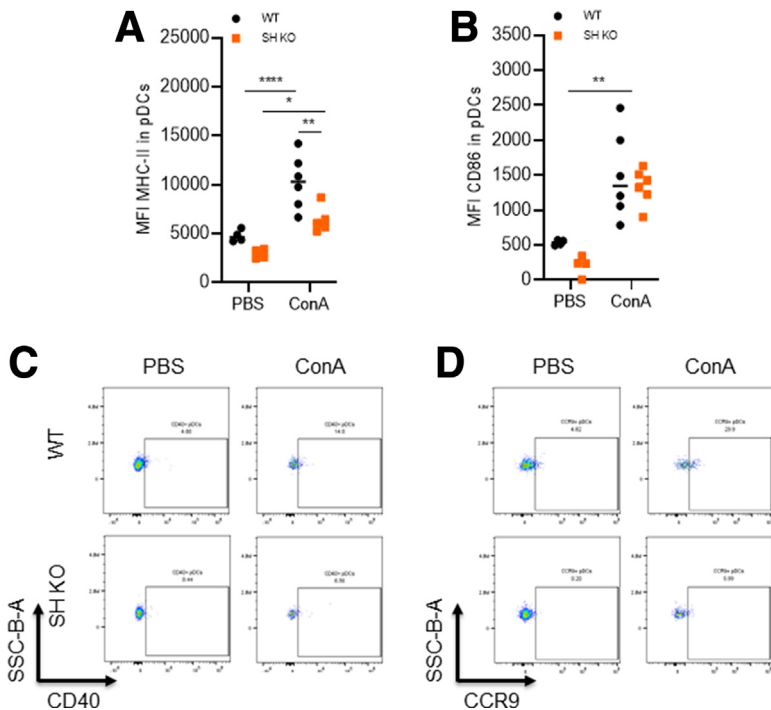


Figure 11. Impaired APC functions and costimulatory molecules in intrahepatic pDCs isolated from SH KO. IHL were analyzed by flow cytometry 6 hours after ConA injection. Detection and analysis of the MFI of (A) MHC-II and (B) CD86 in liver's pDCs. (C, D) Representative FACS plots of frequencies of CD40 and CCR9 markers in liver pDCs. Bars in the scatter plots represent the median value. Statistical analysis was performed with 2-way ANOVA and Tukey post hoc test; * $P < .05$; ** $P < .005$; *** $P < .0005$; **** $P < .00005$.

in mediating immune responses to infections,^{45,46} persistent IFN-I signaling has been associated with autoimmune and inflammatory diseases.⁴⁷ Moreover, we have recently shown that IFN-I enhanced transforming growth factor- β -induced liver fibrosis during HIV infection with antiretroviral therapy.²² However, IL21 expression was significantly elevated in IHL from ConA-treated SH KO mice only while IFN- γ , IFN- β , and OAS1 were not induced when compared with IHL from WT mice (Figure 14 and data not shown). Of note, Stat1 phosphorylation can occur through IFN-I and IFN-II.^{48,49} ConA-induced hepatitis and ALI is reported to be mediated by CD4 T-cell-induced IFN- γ that triggers Stat1 signaling activation and apoptosis in hepatocytes.³⁷ Thus, the lack or low induction of IFN- γ and IFN- β in IHL from SH-null mice could explain the absence of Stat1 phosphorylation in the liver (Figures 5 and 7).

In ConA-mediated hepatitis mouse model, it was reported that IL6-induced Stat3 activation protects against liver injury by suppressing IFN- γ -induced apoptosis in hepatocytes.³⁷ It is important to point out that Stat3 signaling can be activated by various cytokines, including IL6 and IL21.^{50,51} In addition, there is evidence that type I, II, and III IFNs can also activate Stat3 signaling to some extent.^{52,53} However, in this study, IL21 was the only cytokine significantly elevated in the total liver and in the IHL from SH KO mice after treatment (Figures 5H and 14B). IL21 is a highly pleiotropic γ c cytokine primarily produced by CD4 T cells and it affects the differentiation and function of several immune cell types including T, B, and natural killer cells.⁵⁴ Although discrepancies have been reported about the exact role of IL21 in inflammation and disease,⁵⁴ IL21 has

shown a potent antitumor property in mouse tumor models and clinical trials in patients with advanced solid tumors.⁵⁵ Here, we demonstrated that the IL21/Stat3 signaling pathway mediates protection against ALI in SH-deficient mice.

To elucidate how SH-null pDCs enhance tolerance in the liver, we performed a characterization of IHL. In naive mice, we observed that the absence of SH in pDC was associated with immature DC functions of pDCs (MHC-II^{Low}CD86^{Low}CCR9^{Low}CD40^{Low}) (Figure 14), indicating that SH positively regulates these markers and confers to pDCs their APC features. Indeed, CD40-CD40L (CD154) interactions mediate 1 of the most effective APC-activating signals and CD40-signaling blockade is known to prevent T-cell activation to induce tolerance.⁵⁶⁻⁵⁸ Moreover, CCR9 is a gut-homing chemokine receptor highly expressed in pDCs.⁵⁹ Interestingly, Koda et al²⁶ recently showed that CCR9-null pDCs preferentially migrated to the inflamed liver and exerted a more effective immunosuppressive effect. However, we did not observe a higher SH-null pDCs (CCR9^{low}) in the inflamed liver in our study (Figure 10). That could be because, besides CCR9 inhibition, the lack of SH in pDCs also affected the expression of several other molecules involved in APC functions. It will be of interest to define how each molecule reduction in SH-null pDC contributes to the protective effect in the liver.

As observed *in vivo*, in a coculture system, pDCs effectively prevent the activation of CD4 T cells by inhibiting the expression of CD25 and CD69 in T cells. This suppression of CD4 T-cells activity was significantly enhanced by SH-null pDCs (Figure 16). We will decipher in our next study the

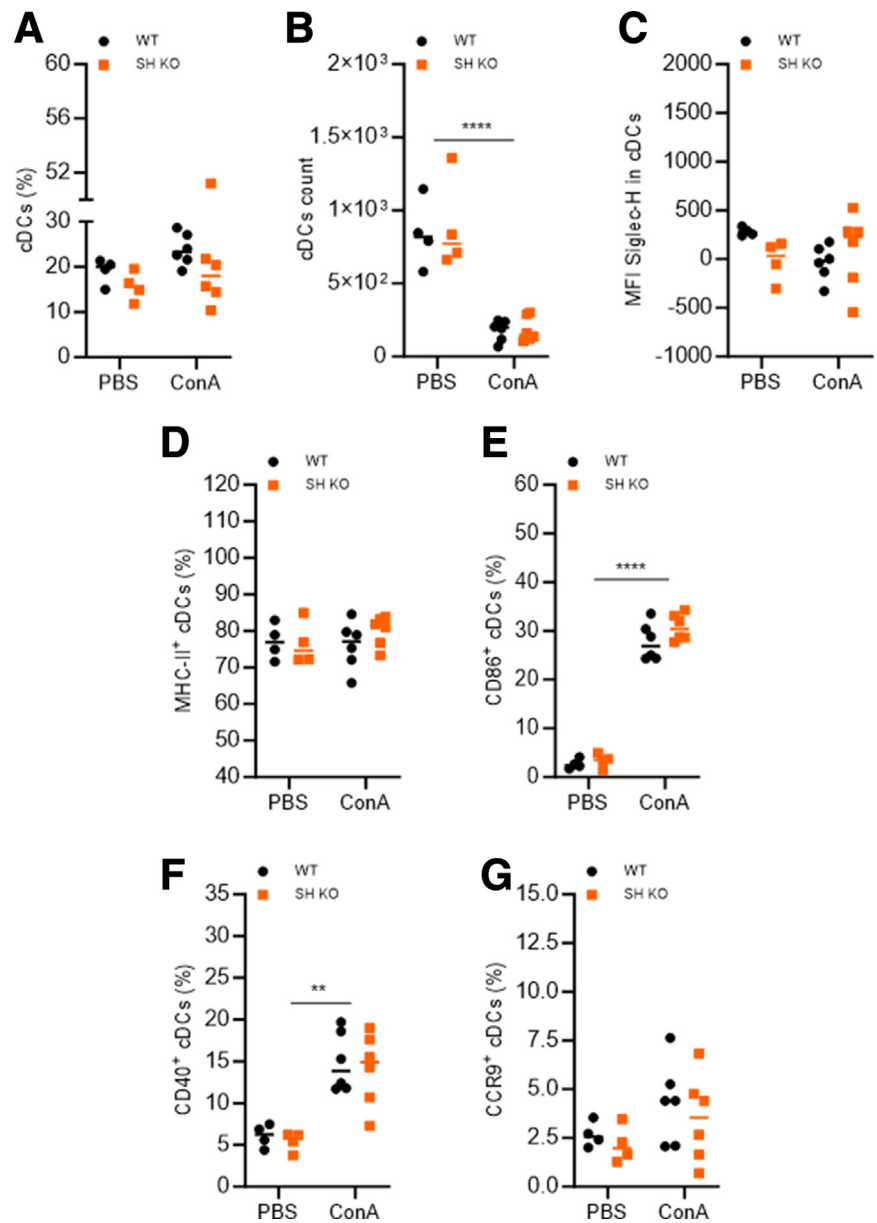


Figure 12. Intrahepatic cDCs and associated costimulatory molecules are modulated similarly in ConA-treated WT and SH KO mice. IHL were analyzed by flow cytometry 6 hours after ConA injection. Detection and analysis of (A, B) frequency and number of cDCs; (C) MFI of SH in cDCs and the percentage of (D-H) MHC-II, CD86, CD40, and CCR9 in liver's pDCs. Bars in the scatter plots represent the median value. Statistical analysis was performed with 2-way ANOVA and Tukey post hoc test; * $P < .05$; ** $P < .005$; *** $P < .0005$; **** $P < .00005$.

associated molecular mechanisms through a deep sequencing analysis of pDCs isolated from naive and inflamed livers.

Specific inhibition of SH in pDCs may seem a beneficial therapeutic approach to protecting against ALI; it is important to point out that SH-deficient pDCs with elevated IFN-I production and impaired APC maturation may potentially aggravate pDC-induced chronic inflammatory diseases including systemic lupus erythematosus,^{36,60} psoriasis,⁶¹ virus infection,^{23,24,41} liver fibrosis, and cancer.

In summary, the present study provides novel mechanistic insights of SH-null pDCs in protecting against acute liver inflammation and disease. Although a human homologue of SH is not known yet, the identification of a human Siglec with similar effects in human pDCs will help to further understand the role of pDCs in human inflammatory

disorders and offer new avenue for potential pDCs-based therapeutic interventions.

Methods

Generation of Genetically Modified Mice, Husbandry, and Treatments

The CRISPR/Cas9 system was used to induce SH genes mutations in C57BL/6 mice as previously described.^{62,63} Briefly, we injected Cas9 and guide RNAs for SH gene and the DAP12-associated SH into C57BL/6 zygotes to generate SH^{-/-} (SH KO) mice. BDCA2 transgenic mice were obtained and used as previously described.³⁴

Male C57BL/6 mice were used throughout the study because male mice are more susceptible to liver diseases than female mice.^{64,65} All the mice were housed in a temperature-

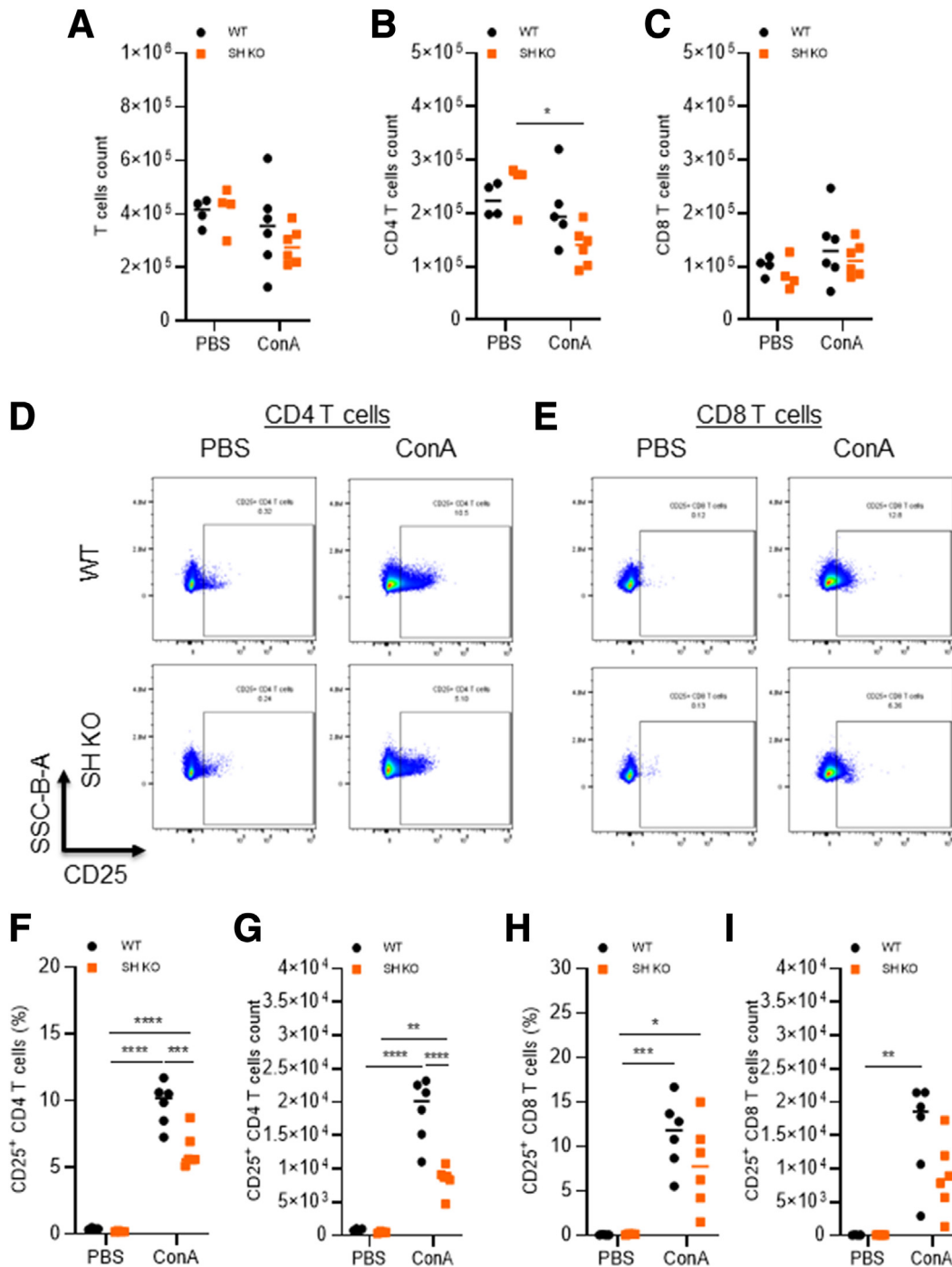


Figure 13. Reduced activation of T cells in the liver of ConA-treated SH deficient mice. IHL were isolated from WT and SH KO mice 6 hours after PBS/ConA administration and analyzed by flow cytometer. (A–C) Intrahepatic total T cells, CD4, and CD8 T cells numbers. (D, E) Representative FACS plots of intrahepatic CD25⁺ CD4 and CD8 T cells. Flow cytometer detection and analysis of the frequencies and cell count of (F, G) CD25⁺CD4 T cells and (H, I) CD25⁺CD8 T cells in the liver. Bars in the scatter plots represent the median value. Statistical analysis was performed with 2-way ANOVA and Tukey post hoc test; **P* < .05; ***P* < .005; ****P* < .0005; *****P* < .00005.

controlled environment ($23 \pm 2^\circ\text{C}$) under a 12-hours light/dark cycle with free access to water and food. All animal studies were approved by the University of Maryland School of Medicine IACUC (AUP-1220008 and AUP-00000478).

Animals were administrated with ConA (15 mg/kg, intravenously) from Sigma Millipore, SAP-conjugated anti-BDCA2 antibody or pDC-dAb (10 $\mu\text{g}/\text{mouse}$, intraperitoneally) for pDCs depletion, InVivoMab antimouse IL21R

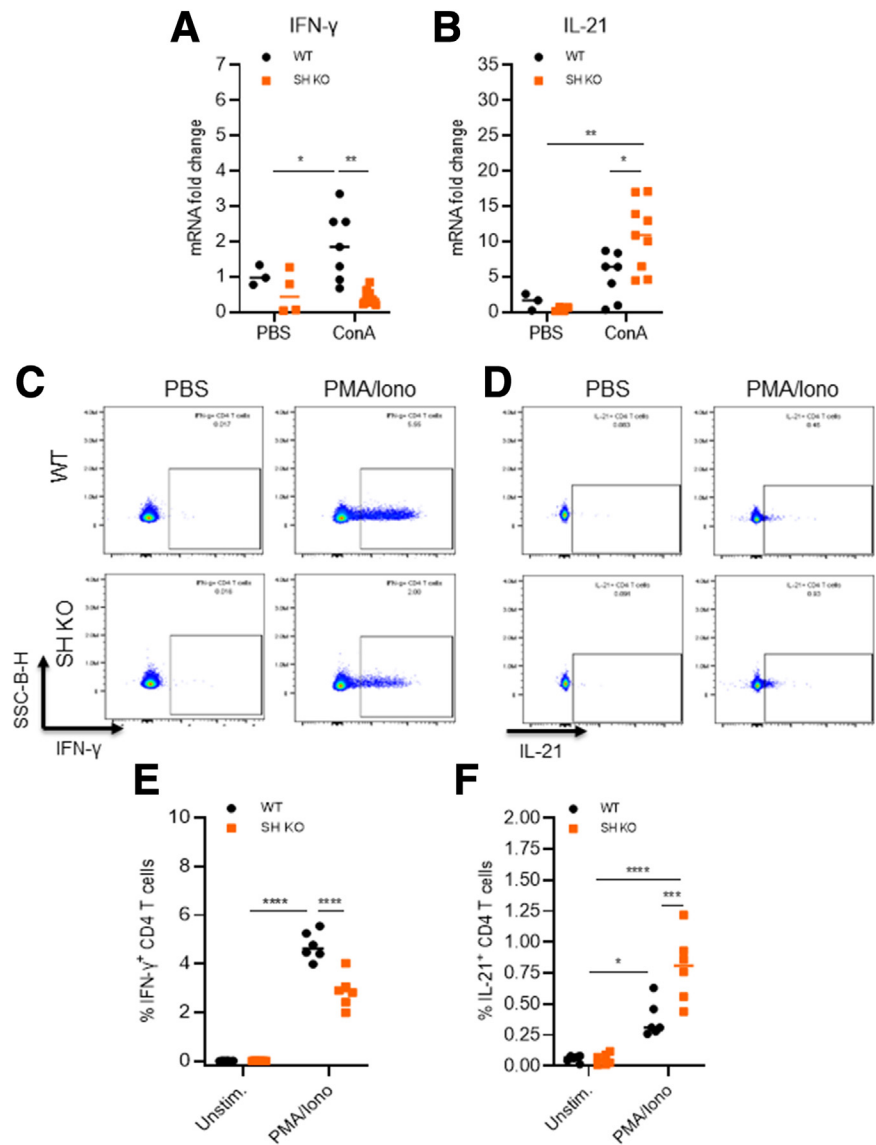


Figure 14. Reduction of IFN- γ /Th1 response and promotion of IL21⁺ CD4 T cells in SH-null mice. (A, B) Real-time quantitative PCR detection of IFN- γ and IL21 mRNAs in the IHL. Splenocytes isolated from WT and SH KO were stimulated with phorbol myristate acetate (PMA) and ionomycin in presence of brefeldin A. (C, D) Representative FACS plots of IFN- γ ⁺ and IL21⁺ CD4 T cells. (E, F) Summarized data showing the frequency of IFN- γ ⁺ and IL21⁺ CD4 T cells. Bars in the scatter plots represent the median value. Statistical analysis was performed with 2-way ANOVA and Tukey post hoc test; * $P < .05$; ** $P < .005$; *** $P < .0005$; **** $P < .00005$.

antibody (1 mg/kg, intraperitoneally) from BioXCell, and Stat3 inhibitor HJC-0416 (10 mg/kg, intraperitoneally) from MedChemExpress. Animals were euthanized up to 12 hours after ConA injection.

RNA Extraction and Real-Time Quantitative PCR

Total RNA was extracted from cells (RNeasy Plus Kit, QIAGEN) and from liver tissues using QIAzol Lysis Reagent and gDNA Eliminator Solution (RNeasy Plus Universal Kits, QIAGEN), and quantified using Nanodrop. 0.2–2 μ g of total RNAs were used for cDNA preparation by reverse transcription with random primers and SuperScript III (Invitrogen), according to the manufacturer's instructions. Two microliters of diluted (1:10) cDNA were used for quantification with the Power SyBR Green PCR Master Mix (Applied Biosystems) on the with CFX Opus 384 Real-Time PCR System from Bio-Rad, using specific mouse primers

(Table 1). The comparative Ct method was used for the analysis of real-time PCR data.^{22,66,67} Data were normalized using mouse GAPDH as the housekeeping gene and expressed as the relative mRNA level compared with the control animals.

Protein Extraction and Immunoblot

Total proteins were extracted from snap-frozen liver tissues using RIPA buffer (Thermo Scientific) with protease and phosphatase inhibitor cocktail (Pierce). Liver protein extracts were quantified by BCA and 20 μ g resolved on sodium dodecyl-sulfate polyacrylamide gel electrophoresis (4%–12%), transferred onto a nitrocellulose membrane and incubated with the following primary antibodies at 1:1000 dilution: phospho-JNK (#4668), phospho-STAT1 Tyr701 (#9167), phospho-STAT3 Tyr705 (#9145), and total JNK (#9252), STAT1 (#14994), STAT3 (#9139), all from Cell

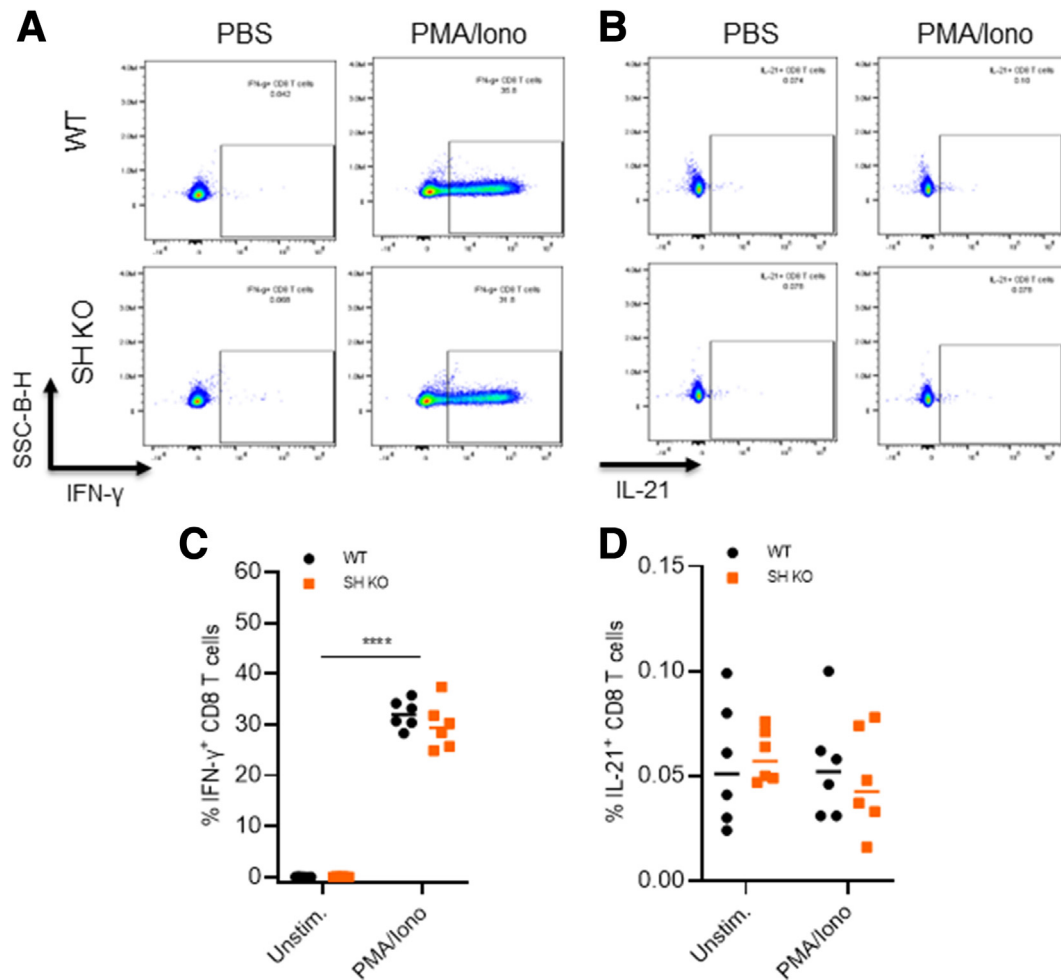


Figure 15. No effect on IFN- γ or IL21 production in SH deficient mice CD8 T cells. WT and SH KO splenocytes were stimulated with phorbol myristate acetate (PMA) and ionomycin with brefeldin A. (A, B) Representative FACS plots of IFN- γ ⁺ CD8 T cells and IL21⁺ CD8 T cells. (C, D) Summarized data showing the frequency of IFN- γ ⁺ CD8 T cells and IL21⁺ CD8 T cells. Bars in the scatter plots represent the median value. Statistical analysis was performed with 2-way ANOVA and Tukey post hoc test; * $P < .05$; ** $P < .005$; *** $P < .0005$; **** $P < .00005$.

Signal; secondary antibodies were either antimouse or antirabbit coupled with horseradish peroxidase. Horseradish peroxidase-conjugated β -actin (1/5000, A3854-200 UL Sigma/Millipore) was used as housekeeping protein. Bands were revealed using the ECL (Millipore and Invitrogen) with BioRad CCD camera and quantified with ImageJ software.

Histology and Immunohistochemistry/ Fluorescence Staining

For immunohistochemical or immunofluorescence staining, paraffin-embedded formalin-fixed liver sections (5 μ m) from mice were stained with hematoxylin and eosin, or with mouse anti-CD45 (#14-0451-85, Invitrogen), anti-CD303 (BDCA2; #DDX043P, Eurobio Scientific) antibodies after antigen retrieval then detected by incubating with a secondary antimouse conjugated with Alexa Fluor 488 (1:500, Invitrogen). TUNEL assay kit was obtained from Roche and liver sections were treated with proteinase and stained following the manufacturer's instructions. Nuclei

were counterstained with Hoechst 33342 (Sigma). All images were acquired with $\times 20$ magnification lens.

Immune Cells Isolation and Flow Cytometry

Immune cells were isolated from the liver as described previously with slight modifications.⁶⁸ Briefly, livers were perfused through the portal vein with a wash buffer (PBS 1x, 2% fetal bovine serum, 1% penicillin/streptomycin, and 0.1 mg/ml DNase I) and then minced with gentleMACS Dissociator in a Liver Digestion Medium (#17703034, ThermoFisher) followed with incubation for 30 minutes at 37°C. The digested liver was mixed with Percoll (40% final) and loaded onto 80% Percoll followed with centrifugation for 30 minutes at 800 g , room temperature with brake off. Immune cells were collected at the interphase and washed. Splens were also processed into splenocytes with gentleMACS Dissociator. Red blood cells were removed with ACK lysis buffer (Invitrogen) and cells resuspended in wash buffer for downstream analysis.

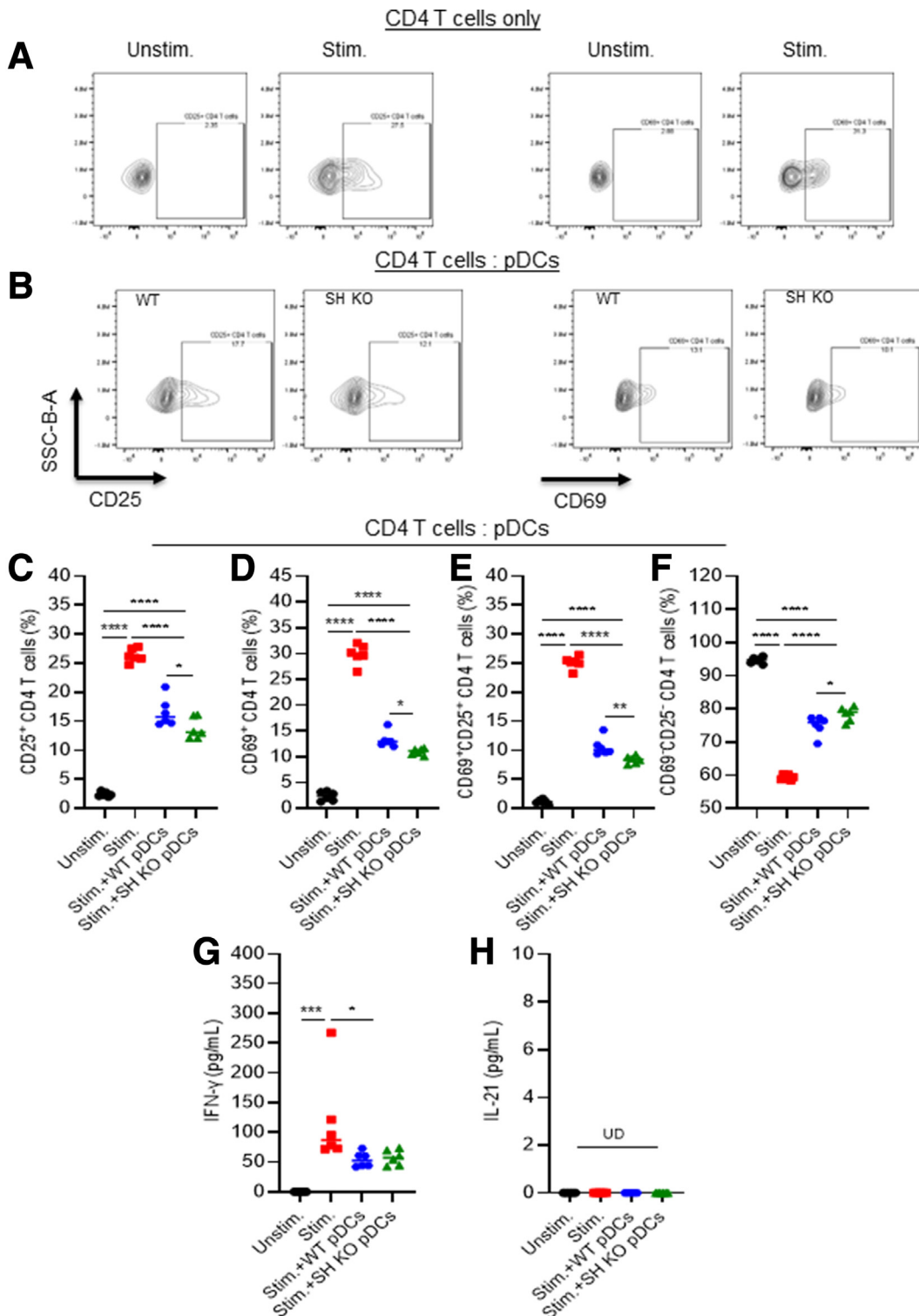


Figure 16. SH deficiency enhances pDC-induced inhibition of CD4 T cells activation in vitro. Purified bone marrow FLT3L-derived pDCs from WT and SH KO mice (7.5×10^4 cells per well) were cocultured with purified naive CD4 T cells (0.3 million cells per well), followed by stimulation with CD3/CD28 microbeads for 72 hours. (A, B) Representative FACS plots of CD25⁺ and CD69⁺ CD4 T cells. Summarized data of the percentage of (C, D) CD25⁺ and CD69⁺ CD4 T cells, and (E, F) double CD69/CD25 positive or negative CD4 T cells. Enzyme-linked immunosorbent assay detection of (G, H) IFN- γ and IL21 concentrations in the culture supernatants. Bars in the scatter plots represent the median value. Statistical analysis was performed with 1-way ANOVA and Tukey post hoc test; * $P < .05$; ** $P < .005$; *** $P < .0005$; **** $P < .00005$.

Table 1. Oligonucleotides/PCR Primers Used in the Study

Primer ID	Forward	Reverse
IL6	GCTACCAAACCTGGATATAATCAGGA	CCAGGTAGCTATGGTACTCCAGAA
TNF- α	GCTGAGCTCAAAACCCCTGGTA	GTTGGTCCCCCTTCTCCA
IFN- γ	AGCAAGGCCGAAAAAGGATGC	TCATTGAATGCTTGGCGCTG
IRF-1	CAGAGGAAAGAGAGAAAGTCC	CACACGGTGACAGTGCTGG
CXCL-10	GATGACGGGCCAGTGAGAAT	CTCAACACGTGGGCAGGATA
SOCS3	GAGATTTTCGCTTCGGGACTA	GGAAACTTGCTGTGGGTGA
IFN- β	CTGGCTTCCATCATGAACAA	CATTTCCGAATGTTCTGTCCT
IL21	CATCATTGACCTCGTGGCCC	ACGAATCACAGGAAGGGCAT
IL1 β	TTCGTGAATGAGCAGACAG	TGGTTTCTTGTGACCCTGAGC
TGF- β	GGTCACCCCGCTGCTAATG	CAGAAGTTGGCATGGTAGCC
IL4	GAACGAGGTCACAGGAGAAG	ACCTTGAAGCCCTACAGA
IL5	GAGATTCCCATGAGCACAGT	CTCCAATGCATAGCTGGTGAT
IL12a	TTAGCCAGTCCCGAAACCTG	TGTCTTCAGCAGTGCAGGAAT
IL15	ACAGCTCAGAGAGGTCAGGA	AGCAAGGACCATGAAGAGGC
IL17	CACCGCAATGAAGACCCTGA	TTCCCTCCGCATTGACACAG
ISG-15	AAGCAGCCAGAAGCAGACTC	GTGACGGACACCAGGAAATC
OAS1	GGCTGAAGAGGCTGATGTGT	CAGTTCTCCTCCACCTGCTC
GAPDH	AGACGGCCGCATCTTCTGTGCA	GCCCAATACGGCCAAATCCGTTT

CXCL-10, C-X-C motif chemokine ligand 10; IFN, interferon; IL, interleukin; IRF-1, interferon regulatory factor 1; SOCS3, suppressor of cytokine signaling-3; TGF, transforming growth factor; TNF, tumor necrosis factor.

Ex vivo T-cell stimulation was performed for 12 hours with phorbol myristate acetate and ionomycin and 9 hours block with brefeldin A. Single-cell suspensions prepared from liver and spleen of mice were stained with surface markers and then fixed and permeabilized with Foxp3/Transcription Factor Staining Buffer Set (eBioscience) for intracellular staining using the following antibodies (Table 2). Cells were then analyzed with a spectral Aurora-UV flow cytometer (CITEK).

Preparation of BM-Derived DCs

BM leukocytes were obtained by hemolysis of BM cell suspensions followed by filtration through a 40- μ m nylon mesh. The cells (20–30 million cells/10-cm dish) were then cultured in pDC-conditioned medium (RPMI 1640, Sigma-Aldrich) containing 10% fetal bovine serum, 1% penicillin/streptomycin, 10 mM HEPES, 1x MEM Non-Essential Amino Acids, 55 μ M 2-mercaptoethanol (Gibco), and 100 ng/mL mouse recombinant FMS-like tyrosine kinase 3 ligand (FLT3L; #550706 BioLegend). After 8 days of culture, cells were harvested and pDCs (CD45⁺/CD11b⁻/B220⁺/PDCA-1⁺) were purified using the EasySep Mouse pDC isolation kit by negative selection (#19764, STEMCELL) following the manufacturer's recommendations. Greater than 80% purity of CD45⁺/CD11b⁻/B220⁺/PDCA-1⁺ cells was confirmed by flow cytometry before subsequent experiments.

In Vitro CD4 T Cell Activation/Suppression Assay

CD25⁻CD4⁺ T cells were isolated from the spleen of WT mice using the MojoSort Mouse CD25⁺CD4⁺ Regulatory T

Cell Isolation Kit (#480137, BioLegend) following the manufacturer's recommendations. A total of 0.25 million WT CD4 T cells with >90% purity were cocultured with 5x10⁴ purified BM FLT3L-derived pDCs from WT and SH KO mice at 1:1/4 ratio as reported previously.^{25,26}

Table 2. Antibodies Used for Flow Cytometry in the Study

Antibody	Supplier	Catalog number
Siglec-H	BioLegend	129610
CD8a	BioLegend	100752
CD45	BioLegend	103136
PDCA-1	BioLegend	127025
CD86	BD Biosciences	564200
CD4	BioLegend	100467
CD11c	BD Biosciences	612796
CCR9	BioLegend	128706
CD3	BioLegend	100259
CD25	BioLegend	102008
NK1.1	BioLegend	108716
B220	BioLegend	103234
CD11b	BioLegend	101228
MHC-II	BioLegend	107622
CD40	BioLegend	124632
IFN- γ	BD Biosciences	564336
IL21	ThermoFisher	17-7211-82
CD69	BioLegend	104537
Zombie NIR	BioLegend	423106

Cocultured cells were stimulated with 2 μ L of Dynabeads mouse T-activator CD3/CD28 (ThermoFisher Scientific) at 37°C for 72 hours. After incubation, the T-cell activation/suppression was assessed using flow cytometry and enzyme-linked immunosorbent assay.

Quantification of Secreted Proteins by Enzyme-Linked Immunosorbent Assay

ALT (#XPEM0829, XpressBio), HA (Echelon Biosciences Inc), IL6 (#M6000B, RND), tumor necrosis factor- α (#MTA00B, RND), IFN- γ (#MIF001, RND), and IL21 (#BMS6021, ThermoFisher Scientific) secretions were detected in plasmas or supernatants and quantified by enzyme-linked immunosorbent assay following the manufacturer's instructions.

Statistical Analysis

Statistical significance was assessed by 2-tailed unpaired Student *t* tests (used to analyzed means in normally distributed populations) or 1- and 2-way analysis of variance (used to analyze ≥ 3 variables) using Prism 10 (GraphPad Software).

References

- Crispe IN. The liver as a lymphoid organ. *Annu Rev Immunol* 2009;27:147–163.
- Dong Z, Wei H, Sun R, et al. The roles of innate immune cells in liver injury and regeneration. *Cell Mol Immunol* 2007;4:241–252.
- Thomson AW, Knolle PA. Antigen-presenting cell function in the tolerogenic liver environment. *Nat Rev Immunol* 2010;10:753–766.
- Antoniades CG, Berry PA, Wendon JA, et al. The importance of immune dysfunction in determining outcome in acute liver failure. *J Hepatol* 2008; 49:845–861.
- Possamai LA, Thursz MR, Wendon JA, et al. Modulation of monocyte/macrophage function: a therapeutic strategy in the treatment of acute liver failure. *J Hepatol* 2014; 61:439–445.
- Heymann F, Tacke F. Immunology in the liver: from homeostasis to disease. *Nat Rev Gastroenterol Hepatol* 2016;13:88–110.
- Siegal FP, Kadowaki N, Shodell M, et al. The nature of the principal type 1 interferon-producing cells in human blood. *Science* 1999;284:1835–1837.
- Kadowaki N, Antonenko S, Lau JY, et al. Natural interferon alpha/beta-producing cells link innate and adaptive immunity. *J Exp Med* 2000;192:219–226.
- Cella M, Jarrossay D, Facchetti F, et al. Plasmacytoid monocytes migrate to inflamed lymph nodes and produce large amounts of type I interferon. *Nat Med* 1999; 5:919–923.
- Barchet W, Cella M, Odermatt B, et al. Virus-induced interferon alpha production by a dendritic cell subset in the absence of feedback signaling in vivo. *J Exp Med* 2002;195:507–516.
- Tel J, Lambeck AJ, Cruz LJ, et al. Human plasmacytoid dendritic cells phagocytose, process, and present exogenous particulate antigen. *J Immunol* 2010; 184:4276–4283.
- Di Pucchio T, Chatterjee B, Smed-Sorensen A, et al. Direct proteasome-independent cross-presentation of viral antigen by plasmacytoid dendritic cells on major histocompatibility complex class I. *Nat Immunol* 2008; 9:551–557.
- Salio M, Palmowski MJ, Atzberger A, et al. CpG-matured murine plasmacytoid dendritic cells are capable of in vivo priming of functional CD8 T cell responses to endogenous but not exogenous antigens. *J Exp Med* 2004; 199:567–579.
- Boonstra A, Asselin-Paturel C, Gilliet M, et al. Flexibility of mouse classical and plasmacytoid-derived dendritic cells in directing T helper type 1 and 2 cell development: dependency on antigen dose and differential toll-like receptor ligation. *J Exp Med* 2003; 197:101–109.
- Yu CF, Peng WM, Oldenburg J, et al. Human plasmacytoid dendritic cells support Th17 cell effector function in response to TLR7 ligation. *J Immunol* 2010; 184:1159–1167.
- Ito T, Yang M, Wang YH, et al. Plasmacytoid dendritic cells prime IL-10-producing T regulatory cells by inducible costimulator ligand. *J Exp Med* 2007;204:105–115.
- Moseman EA, Liang X, Dawson AJ, et al. Human plasmacytoid dendritic cells activated by CpG oligodeoxynucleotides induce the generation of CD4+CD25+ regulatory T cells. *J Immunol* 2004;173:4433–4442.
- Kawamura K, Kadowaki N, Kitawaki T, et al. Virus-stimulated plasmacytoid dendritic cells induce CD4+ cytotoxic regulatory T cells. *Blood* 2006;107:1031–1038.
- Eloranta ML, Alm GV, Ronnblom L. Disease mechanisms in rheumatology—tools and pathways: plasmacytoid dendritic cells and their role in autoimmune rheumatic diseases. *Arthritis Rheum* 2013;65:853–863.
- Pang L, Yeung OWH, Ng KTP, et al. Postoperative plasmacytoid dendritic cells secrete IFN α to promote recruitment of myeloid-derived suppressor cells and drive hepatocellular carcinoma recurrence. *Cancer Res* 2022;82:4206–4218.
- Li S, Wu J, Zhu S, et al. Disease-associated plasmacytoid dendritic cells. *Front Immunol* 2017;8:1268.
- Ahodantin J, Nio K, Funaki M, et al. Type I interferons and TGF- β cooperate to induce liver fibrosis during HIV-1 infection under antiretroviral therapy. *JCI Insight* 2022;7.
- Li G, Cheng M, Nunoya J, et al. Plasmacytoid dendritic cells suppress HIV-1 replication but contribute to HIV-1 induced immunopathogenesis in humanized mice. *PLoS Pathog* 2014;10:e1004291.
- Li G, Zhao J, Cheng L, et al. HIV-1 infection depletes human CD34+CD38- hematopoietic progenitor cells via pDC-dependent mechanisms. *PLoS Pathog* 2017;13: e1006505.
- Koda Y, Nakamoto N, Chu PS, et al. Plasmacytoid dendritic cells protect against immune-mediated acute liver injury via IL-35. *J Clin Invest* 2019;129:3201–3213.

26. Koda Y, Nakamoto N, Chu PS, et al. CCR9 axis inhibition enhances hepatic migration of plasmacytoid DCs and protects against liver injury. *JCI Insight* 2022;7.
27. Blasius AL, Cella M, Maldonado J, et al. Siglec-H is an IPC-specific receptor that modulates type I IFN secretion through DAP12. *Blood* 2006;107:2474–2476.
28. Zhang J, Raper A, Sugita N, et al. Characterization of Siglec-H as a novel endocytic receptor expressed on murine plasmacytoid dendritic cell precursors. *Blood* 2006;107:3600–3608.
29. Leylek R, Alcantara-Hernandez M, Lanzar Z, et al. Integrated cross-species analysis identifies a conserved transitional dendritic cell population. *Cell Rep* 2019;29:3736–3750 e8.
30. Sulczewski FB, Maqueda-Alfaro RA, Alcantara-Hernandez M, et al. Transitional dendritic cells are distinct from conventional DC2 precursors and mediate proinflammatory antiviral responses. *Nat Immunol* 2023;24:1265–1280.
31. Lutz K, Musumeci A, Sie C, et al. Ly6D(+)Siglec-H(+) precursors contribute to conventional dendritic cells via a Zbtb46(+)Ly6D(+) intermediary stage. *Nat Commun* 2022;13:3456.
32. Takagi H, Fukaya T, Eizumi K, et al. Plasmacytoid dendritic cells are crucial for the initiation of inflammation and T cell immunity in vivo. *Immunity* 2011;35:958–971.
33. Cheng L, Li G, Pellegry CM, et al. TLR9- and CD40-targeting vaccination promotes human B cell maturation and IgG induction via pDC-dependent mechanisms in humanized mice. *Front Immunol* 2021;12:672143.
34. Chappell CP, Giltiay NV, Draves KE, et al. Targeting antigens through blood dendritic cell antigen 2 on plasmacytoid dendritic cells promotes immunologic tolerance. *J Immunol* 2014;192:5789–5801.
35. Mandl M, Drechsler M, Jansen Y, et al. Evaluation of the BDCA2-DTR transgenic mouse model in chronic and acute inflammation. *PLoS One* 2015;10:e0134176.
36. Schmitt H, Sell S, Koch J, et al. Siglec-H protects from virus-triggered severe systemic autoimmunity. *J Exp Med* 2016;213:1627–1644.
37. Hong F, Jaruga B, Kim WH, et al. Opposing roles of STAT1 and STAT3 in T cell-mediated hepatitis: regulation by SOCS. *J Clin Invest* 2002;110:1503–1513.
38. Leonard WJ, Zeng R, Spolski R. Interleukin 21: a cytokine/cytokine receptor system that has come of age. *J Leukoc Biol* 2008;84:348–356.
39. Zeng R, Spolski R, Casas E, et al. The molecular basis of IL-21-mediated proliferation. *Blood* 2007;109:4135–4142.
40. Wan CK, Andraski AB, Spolski R, et al. Opposing roles of STAT1 and STAT3 in IL-21 function in CD4+ T cells. *Proc Natl Acad Sci U S A* 2015;112:9394–9399.
41. Szumilas N, Corneth OBJ, Lehmann CHK, et al. Siglec-H-deficient mice show enhanced type I IFN responses, but do not develop autoimmunity after influenza or LCMV infections. *Front Immunol* 2021;12:698420.
42. Ulsenheimer A, Gerlach JT, Jung MC, et al. Plasmacytoid dendritic cells in acute and chronic hepatitis C virus infection. *Hepatology* 2005;41:643–651.
43. Beckebaum S, Zhang X, Chen X, et al. Increased levels of interleukin-10 in serum from patients with hepatocellular carcinoma correlate with profound numerical deficiencies and immature phenotype of circulating dendritic cell subsets. *Clin Cancer Res* 2004;10:7260–7269.
44. Pedroza-Gonzalez A, Zhou G, Vargas-Mendez E, et al. Tumor-infiltrating plasmacytoid dendritic cells promote immunosuppression by Tr1 cells in human liver tumors. *Oncoimmunology* 2015;4:e1008355.
45. Gilliet M, Cao W, Liu YJ. Plasmacytoid dendritic cells: sensing nucleic acids in viral infection and autoimmune diseases. *Nat Rev Immunol* 2008;8:594–606.
46. Swiecki M, Gilfillan S, Vermi W, et al. Plasmacytoid dendritic cell ablation impacts early interferon responses and antiviral NK and CD8(+) T cell accrual. *Immunity* 2010;33:955–966.
47. Barrat FJ, Su L. A pathogenic role of plasmacytoid dendritic cells in autoimmunity and chronic viral infection. *J Exp Med* 2019;216:1974–1985.
48. Liu S, Imani S, Deng Y, et al. Targeting IFN/STAT1 pathway as a promising strategy to overcome radio-resistance. *Onco Targets Ther* 2020;13:6037–6050.
49. Plataniias LC. Mechanisms of type-I- and type-II-interferon-mediated signalling. *Nat Rev Immunol* 2005;5:375–386.
50. West PK, McCorkindale AN, Guennewig B, et al. The cytokines interleukin-6 and interferon-alpha induce distinct microglia phenotypes. *J Neuroinflammation* 2022;19:96.
51. Witalisz-Siepracka A, Klein K, Zdarsky B, et al. The multifaceted role of STAT3 in NK-cell tumor surveillance. *Front Immunol* 2022;13:947568.
52. Dimberg LY, Dimberg A, Ivarsson K, et al. Stat1 activation attenuates IL-6 induced Stat3 activity but does not alter apoptosis sensitivity in multiple myeloma. *BMC Cancer* 2012;12:318.
53. Tsai MH, Pai LM, Lee CK. Fine-tuning of type I interferon response by STAT3. *Front Immunol* 2019;10:1448.
54. Spolski R, Leonard WJ. Interleukin-21: a double-edged sword with therapeutic potential. *Nat Rev Drug Discov* 2014;13:379–395.
55. Skak K, Kragh M, Hausman D, et al. Interleukin 21: combination strategies for cancer therapy. *Nat Rev Drug Discov* 2008;7:231–240.
56. Grewal IS, Xu J, Flavell RA. Impairment of antigen-specific T-cell priming in mice lacking CD40 ligand. *Nature* 1995;378:617–620.
57. Borrow P, Tishon A, Lee S, et al. CD40L-deficient mice show deficits in antiviral immunity and have an impaired memory CD8+ CTL response. *J Exp Med* 1996;183:2129–2142.
58. Diehl L, Den Boer AT, van der Voort EI, et al. The role of CD40 in peripheral T cell tolerance and immunity. *J Mol Med (Berl)* 2000;78:363–371.
59. Wendland M, Czeloth N, Mach N, et al. CCR9 is a homing receptor for plasmacytoid dendritic cells to the small intestine. *Proc Natl Acad Sci U S A* 2007;104:6347–6352.
60. Huang X, Dorta-Estremera S, Yao Y, et al. Predominant role of plasmacytoid dendritic cells in

- stimulating systemic autoimmunity. *Front Immunol* 2015;6:526.
61. Albanesi C, Scarponi C, Bosisio D, et al. Immune functions and recruitment of plasmacytoid dendritic cells in psoriasis. *Autoimmunity* 2010;43:215–219.
 62. Wang H, Yang H, Shivalila CS, et al. One-step generation of mice carrying mutations in multiple genes by CRISPR/Cas-mediated genome engineering. *Cell* 2013;153:910–918.
 63. Wang X, Liu M, Zhang J, et al. CD24-Siglec axis is an innate immune checkpoint against metaflammation and metabolic disorder. *Cell Metab* 2022;34:1088–1103 e6.
 64. Naugler WE, Sakurai T, Kim S, et al. Gender disparity in liver cancer due to sex differences in MyD88-dependent IL-6 production. *Science* 2007;317:121–124.
 65. Hwang LL, Wang CH, Li TL, et al. Sex differences in high-fat diet-induced obesity, metabolic alterations and learning, and synaptic plasticity deficits in mice. *Obesity (Silver Spring)* 2010;18:463–469.
 66. Ahodantin J, Bou-Nader M, Cordier C, et al. Hepatitis B virus X protein promotes DNA damage propagation through disruption of liver polyploidization and enhances hepatocellular carcinoma initiation. *Oncogene* 2019;38:2645–2657.
 67. Ahodantin J, Lekbaby B, Bou Nader M, et al. Hepatitis B virus X protein enhances the development of liver fibrosis and the expression of genes associated with epithelial-mesenchymal transitions and tumor progenitor cells. *Carcinogenesis* 2020;41:358–367.
 68. Xiong X, Kuang H, Ansari S, et al. Landscape of inter-cellular crosstalk in healthy and NASH liver revealed by single-cell secretome gene analysis. *Mol Cell* 2019;75:644–660 e5.

Received February 29, 2024. Accepted May 31, 2024.

Correspondence

Address correspondence to: Correspondences. James Ahodantin, PhD, Institute of Human Virology, Division of Virology, Baltimore, Maryland 21201-1544. e-mail: jahodantin@ihv.umaryland.edu; or Lishan Su, PhD, Institute of Human Virology, University of Maryland School of Medicine, Baltimore, Maryland 21201-1544. e-mail: lsu@ihv.umaryland.edu.

Acknowledgments

The authors thank the Su laboratory members including Weirong Yuan, Yichen Lu, and Sahra Sharifi for technical support. They also thank the Institute of Human Virology Animal care facility, and the UMGCCC flow cytometry cores at the University of Maryland School of Medicine.

The authors thank the flow cytometry Shared Service of the University of Maryland Marlene and Stewart Greenebaum Comprehensive Cancer Center for providing the service.

CRedit Authorship Contributions

James Ahodantin, PhD (Conceptualization: Lead; Data curation: Lead; Formal analysis: Lead; Investigation: Lead; Methodology: Lead; Writing – original draft: Lead; Writing – review & editing: Lead)

Jiapeng Wu, MS (Formal analysis: Supporting; Investigation: Supporting; Validation: Supporting; Visualization: Supporting)

Masaya Funaki, MD (Formal analysis: Supporting; Investigation: Supporting; Validation: Supporting; Visualization: Supporting)

Jair Flores, MS (Formal analysis: Supporting; Validation: Supporting; Visualization: Supporting)

Xu Wang, PhD (Formal analysis: Supporting; Validation: Supporting)

Pan Zheng, PhD (Resources: Supporting; Visualization: Supporting)

Yang Liu, PhD (Resources: Supporting; Validation: Supporting)

Lishan Su, PhD (Conceptualization: lead; Funding acquisition: Lead; Writing – review & editing: lead)

Conflicts of interest

The authors disclose no conflicts.

Funding

This study was supported in part by the National Institutes of Health grants #R01DK119937 and #R01AI154722 to Lishan Su and the National Cancer Institute - Cancer Center Support Grant (CCSG) – P30CA134274 to Kevin Cullen.